

Chiral gravitational waves from multi-phase magnetogenesis

H. V. Ragavendra^{a,b}, Gianmassimo Tasinato^{c,d}, and L. Sriramkumar^e

^a*Dipartimento di Fisica e Astronomia “Galileo Galilei”, Università degli Studi di Padova,
Via Marzolo 8, I-35131 Padova, Italy*

^b*Istituto Nazionale di Fisica Nucleare (INFN), Sezione di Padova, Via Marzolo 8, I-35131 Padova, Italy*

^c*Physics Department, Swansea University, SA2 8PP, UK*

^d*Dipartimento di Fisica e Astronomia, Università di Bologna,*

INFN, Sezione di Bologna, viale B. Pichat 6/2, 40127 Bologna, Italy

^e*Centre for Strings, Gravitation and Cosmology, Department of Physics,*

Indian Institute of Technology Madras, Chennai 600036, India

Abstract

Cosmological vector fields are central to many early-Universe phenomena, including inflationary dynamics, primordial magnetogenesis, and dark-matter scenarios. However, constructing models able to generate cosmological magnetic fields while avoiding strong coupling, backreaction, and cosmic microwave background constraints remains challenging. We study a novel mechanism in which brief non-slow-roll phases during inflation amplify primordial magnetic fields at small scales, while maintaining theoretical consistency and observational viability. We incorporate parity-violating interactions in the vector sector and demonstrate, for the first time in a non-slow-roll framework, that chirality can significantly boost magnetic-field amplitudes and imprint distinctive polarization-dependent spectral features. We complement detailed numerical computations with an analytical treatment yielding compact expressions for chiral vector mode functions that reproduce the main spectral properties. We then develop a systematic formalism to evaluate the stochastic gravitational-wave background naturally induced at second order by these amplified fields, identifying both an intensity component and a circularly polarized contribution with characteristic frequency profiles. We discuss detection prospects with future multiband gravitational-wave observatories, showing that chiral signatures could provide a distinctive observational probe. Our results introduce new avenues for enhancing primordial magnetic fields and their associated gravitational-wave signals, opening promising possibilities for their future detection and interpretation, both with cosmological and gravitational wave probes.

1 Introduction

Cosmological vector fields play a central role in a wide range of early-Universe phenomena, from models of inflation (see e.g. [1] for a review) to scenarios of primordial magnetogenesis (see [2–14] for seminal works) and dark-matter models (see e.g. [15]). In particular, primordial magnetogenesis provides an appealing mechanism to account for the large-scale magnetic fields observed in galaxies and clusters. However, concrete realizations face significant theoretical and observational challenges, including strong-coupling regimes, backreaction effects, and bounds from the cosmic microwave background (CMB); see e.g. [16, 17] for reviews. Developing scenarios that overcome these obstacles while still producing observable magnetic fields remains an important open problem.

In this work we explore a novel framework designed to amplify small-scale primordial magnetic fields while simultaneously generating chirality and satisfying both observational constraints (notably those from the CMB) and theoretical consistency requirements such as backreaction control. Our mechanism exploits a brief phase of departure of the inflaton from slow-roll evolution, which can influence the effective couplings between scalar and vector sectors. Such non-slow-roll evolutions are known to enhance the spectrum of curvature perturbations—potentially leading to primordial black-hole formation (see e.g. [18] for a review)—and can likewise be used to boost inflationary magnetic fields. For the first time within a non-slow-roll setting, we consistently incorporate parity-violating effects in the vector sector and show that they can provide an additional and significant enhancement of the magnetic-field amplitude beyond

that produced by the background dynamics alone, as well as adding new features to the magnetic field profile.

After introducing the set-up in Section 2, we perform in Section 3 a detailed numerical analysis of the resulting magnetic-field spectrum. We demonstrate that the spectrum grows from large to small scales, extending and refining previous studies [19–21] of its growth properties. We also show that this behavior allows the model to evade both backreaction constraints and current CMB bounds. We then include parity-violating interactions and find that chirality significantly modifies the spectral shape, generating additional polarization-dependent peaks whose features distinguish the two helicity states. In Section 4 we complement the numerical study with an analytical approach based on [22, 23], deriving compact formulas for the chiral vector mode functions. Despite their simplicity, these expressions successfully reproduce the main characteristics of the full numerical spectra obtained in Section 3.

In Section 5 we develop a systematic framework to compute the stochastic gravitational-wave background (SGWB) induced at second order by the enhanced magnetic fields on small scales. We show that the resulting energy-density spectrum can be decomposed into a standard contribution Ω_{GW} , governed by the total GW intensity, and a parity-violating component Ω_{GW}^V associated with circular polarization. Both contributions exhibit distinctive spectral shapes that can lead to observable signatures. We discuss prospects for detection and characterization with future multiband gravitational-wave observatories, emphasizing that chirality could be inferred from characteristic spectral features. Overall, our scenario provides new mechanisms for enhancing the GW signal and endowing it with properties that may facilitate its detection and interpretation.

2 Our set-up

Our work aims to develop both a numerical and analytical understanding of the properties of chiral magnetic fields generated during inflationary scenarios featuring a departure from slow-roll evolution. As we shall learn, a transient non-slow-roll epoch can lead to a significant rapid amplification of magnetic fields at small scales. This enhancement has important consequences for the generation of a background of chiral gravitational waves after inflation ends, which are sourced by the amplified magnetic field spectrum.

We work in a Friedmann–Lemaître–Robertson–Walker (FLRW) background (with a mostly-plus signature) and we denote conformal time by τ . The dynamics of the electromagnetic field during inflation is governed by the action [24, 25]

$$S[A^\mu] = -\frac{1}{4} \int d\tau d^3x \sqrt{-g} J^2 \left[F_{\mu\nu} F^{\mu\nu} - \frac{\gamma}{2} F_{\mu\nu} \tilde{F}^{\mu\nu} \right], \quad (2.1)$$

where the electromagnetic field strength tensor is defined in terms of the vector potential as $F_{\mu\nu} = \partial_\mu A_\nu - \partial_\nu A_\mu$. Its dual is given by

$$\tilde{F}^{\mu\nu} \equiv \frac{1}{\sqrt{-g}} \epsilon^{\mu\nu\alpha\beta} F_{\alpha\beta}, \quad (2.2)$$

with $\epsilon^{\mu\nu\alpha\beta}$ the totally antisymmetric Levi–Civita tensor. The function J , if dependent on coordinates, breaks the conformal invariance of the electromagnetic action allowing for vector-field amplification, while the parameter γ controls the strength of parity violation in the vector sector.

During inflation, both J and γ are typically modelled as functions of the inflaton or of a spectator field, leading to direct couplings between scalar degrees of freedom and the electromagnetic field strength [19, 20, 25–33]. In scenarios that include brief non-slow-roll phases – often motivated by primordial black hole production (see, e.g. [34] for a review), or by punctuated inflation models [35, 36] – the scalar field velocities may vary rapidly over short time intervals. This behaviour induces *sharp time variations* in both J and γ during the inflationary process. Besides magnetogenesis, such scenarios are useful for building models of longitudinal vector dark matter [37]. In our set-up, without committing to explicit model building, we treat these quantities as explicit functions of conformal time τ . We analyze two representative scenarios

that capture their evolution in the presence of brief non-slow-roll epochs, during which the profiles of J and γ can change significantly.

We work in the Coulomb gauge setting $A_0 = \partial_i A^i = 0$. We introduce the quantity $\mathcal{A}_k = J A_k$, where A_k is the mode function in Fourier space, so that its corresponding equation of motion is [19, 20, 24]

$$\mathcal{A}_k^{\lambda''} + \left(k^2 + 2\lambda\gamma k \frac{J'}{J} - \frac{J''}{J} \right) \mathcal{A}_k^\lambda = 0, \quad (2.3)$$

where the index of polarization is $\lambda = [L, R] = \pm 1$, and a prime indicates derivative along conformal time. While the term $J''/J \propto \tau^{-2}$ introduces a demarcation of sub-Hubble and super-Hubble behavior to the mode function, the term $2\lambda\gamma k J'/J$ induces chiral imbalance, enhancing the mode function of one polarization, while suppressing the other. The exact time, scale and chiral dependence of the effects of these terms is associated with the behavior of $J(\tau)$. The magnetic power spectrum $\mathcal{P}_B^\lambda(k)$ for a given polarization index λ is then [8, 25, 28]

$$\mathcal{P}_B^\lambda(k) = \frac{J^2}{a^4} \frac{k^5}{2\pi^2} |A_k^\lambda|^2 = \frac{k^5}{2\pi^2 a^4} |\mathcal{A}_k^\lambda|^2, \quad (2.4)$$

which is evaluated at the end of inflation, when J is set to reach unity, restoring conformal invariance. For reference, the parity-preserving case ($\gamma = 0$) with monotonic evolution of $J = (a^2/a_e^2)$ throughout inflation (with a_e being the scale factor at the end of inflation) leads to equal and scale-invariant magnetic field spectra for both helicities as [19, 33]

$$\mathcal{P}_B^L(k) = \mathcal{P}_B^R(k) = \frac{9H^4}{8\pi^2}. \quad (2.5)$$

For $\gamma = 0$ we shall denote as \mathcal{P}_B^0 the corresponding total power spectrum $\mathcal{P}_B^{\gamma \rightarrow 0}(k) = \mathcal{P}_B^L(k) + \mathcal{P}_B^R(k) = 9H^4/(4\pi^2)$, and use it as a reference to contrast against the features induced due to deviating phase of J and/or parity-violation ($\gamma \neq 0$), which is the topic we are mostly interested in.

In fact, we now pass to discuss two complementary scenarios of inflationary magnetogenesis, differing in the behaviour of γ as a function of time. In Section 3 we investigate a first scenario, in which we extend the analysis of Ref. [21] by accounting for the finite duration of the non-slow-roll epoch, and by including parity-violating effects through the parameter γ appearing in Eq. (2.1). We make the hypothesis that γ is a constant parameter turned on during the entire inflationary epoch. Our study of this case relies on a numerical analysis of the coupled mode equations, and it reveals new non-trivial features in the profile of the resulting magnetic field spectrum. The second scenario, discussed in Section 4, further generalizes [21] by incorporating parity violation in a setup that remains analytically tractable. In this case, we assume that γ is switched on *only* during the brief non-slow-roll phase. We then derive a fully analytic expression for the gauge-field mode functions, as well as for the chiral magnetic field power spectrum. The interesting implications of both scenarios for the generation of chiral induced gravitational waves are developed in Section 5.

3 First scenario, and numerical analysis

In the first scenario, we model the behavior of the non-conformal coupling function J as often done in models of inflation with a brief phase of ultra slow roll (USR) sandwiched between slow-roll evolutions – see e.g. the review [34] and references therein. We model the time evolution of J as involving three phases, such as $J(\tau) \sim \tau^{-2}, \tau^{-n_2}, \tau^{-2}$. The phases of $J \propto \tau^{-2}$ shall lead to scale-invariant $\mathcal{P}_B(k)$, while the intermediate phase shall lead to deviations from scale-invariance. We may expect such a behavior of J when it is modelled in terms of the inflaton ϕ or the associated kinetic term $X = -\partial_\mu \phi \partial^\mu \phi/2$ in USR models or models that have brief departure from slow-roll evolution (see, for related efforts [20, 27, 33]).

The exact form of $J(\tau)$ can be arrived at by matching conditions at transitions between phases, while ensuring continuity of the function:

$$J(\tau) = \begin{cases} \left(\frac{\tau_e}{\tau_2}\right)^2 \left(\frac{\tau_1}{\tau_2}\right)^{-n_2} \left(\frac{\tau}{\tau_1}\right)^{-2} & \text{for } \tau < \tau_1, \\ \left(\frac{\tau_e}{\tau_2}\right)^2 \left(\frac{\tau}{\tau_2}\right)^{-n_2} & \text{for } \tau_1 < \tau < \tau_2, \\ \left(\frac{\tau}{\tau_e}\right)^{-2} & \text{for } \tau > \tau_2, \end{cases} \quad (3.1)$$

where τ_1 and τ_2 are the times demarcating the phase junctions. We approximate the transition between the three phases as instantaneous. We ensure that $J(\tau)$ is continuous across phases and set $J(\tau_e) = 1$ at the end of inflation τ_e . The setup is very similar to the construction presented in [21]. The difference in the scenario of this section is that here the intermediate phase is not instantaneous but of finite duration, and the index describing the phase n_2 is of finite value. This fact has interesting consequences for phenomenology. For numerical purposes, we describe the transitions through a step function modelled using a hyperbolic tangent function in terms of e-folds $N \equiv \ln(a/a(\tau_e))$.

We solve the electromagnetic mode function numerically in terms of e-folds N for the three-phase model of J and compute the corresponding $\mathcal{P}_B(k)$ at the end of inflation. For carrying on numerics, the inflationary background dynamics can effectively be set as de Sitter expansion, parameterized by a constant Hubble parameter H . The scale factor is then $a(\tau) = -1/(H\tau)$, with $\tau < 0$ during inflation.

3.1 Non-helical case: steepest n_B

First, we analyze the three-phase model in the parity-preserving case ($\gamma = 0$), focusing on the steepest possible growth of $\mathcal{P}_B(k)$. This question is also of interest in comparison with the scalar case. For curvature perturbations, the growing mode during non-slow-roll evolution is well described by a power-law spectrum with spectral index $n \simeq 4$, which represents the maximal slope attainable within this class of scenarios [38, 39].

In contrast, the amplification of vector fluctuations exhibits a more intricate behavior. Although the magnetic power spectrum also grows steeply, with an effective spectral index initially close to $n \simeq 4$, its evolution is not accurately described by a pure power law. Instead, the slope can exceed that of the scalar case, reaching a maximal value of $n \simeq 4.75$, as derived analytically in [21] under the assumption of an infinitesimally brief departure from slow roll. Here we show that even larger values of n can be obtained when the non-slow-roll phase has a finite duration.

Specifically, we numerically analyze a setup featuring a short intermediate non-slow-roll phase of J with a large power-law index τ^{n_2} , following the construction of [21]. We characterize this intermediate stage by large negative values $n_2 \in [-20, -26]$ and a brief duration $\Delta N_2 \leq 0.5$. For these parameters we compute $\mathcal{P}_B(k)$ and the corresponding spectral index $n_B \equiv \frac{d \ln \mathcal{P}_B(k)}{d \ln k}$ numerically, scanning the parameter space to determine the largest attainable value of n_B .

Figure 1 shows that n_B can reach values as high as 5 for $n_2 \in [-20, -26]$ and $\Delta N_2 \gtrsim 0.4$. This slightly exceeds the analytic maximum $n_B = 4.75$ obtained in [21]. The discrepancy between the analytic and numerical maxima can be attributed to the finite duration ΔN_2 of the intermediate phase. Notably, a steeper spectral growth is phenomenologically advantageous when confronting the model with observations, as it more readily evades CMB constraints [16].

3.2 Magnetic power spectrum - the parity-violating case

We proceed to study the three-phase model of J with inclusion of the parity-violation in the action. This is an important new ingredient of our work. See also [26, 29, 31, 32]. In the first scenario of this section we keep the parameter γ constant during inflation. Our fiducial values for the parameters are as follows. The parity-violating term in the action is set to $\gamma = 1$; the onset of intermediate phase to $N_1 = 15$ (counted from the end of inflation); the duration of the phase to $\Delta N_2 = 3$; and the index to $n_2 = -3$. Note that

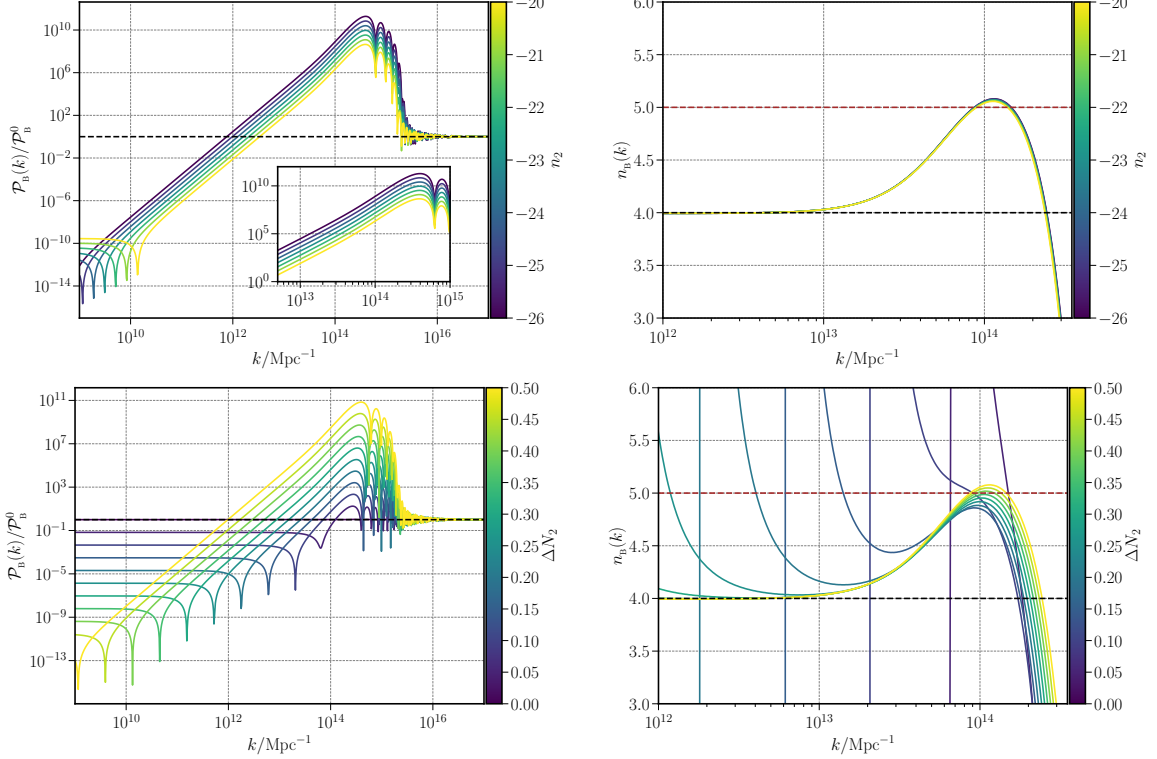


Figure 1: The magnetic power spectrum $\mathcal{P}_B(k)$ (in terms of \mathcal{P}_B^0) and the associated spectral index n_B arising from the three-phase model of $J(N)$ are presented across variations of the parameters characterizing the intermediate phase, namely n_2 and ΔN_2 . We compute them in the parity-preserving case of $\gamma = 0$ with a representative value of $N_1 = 15$ (counted from the end of inflation). For reference, we mark the value of $\mathcal{P}_B(k) = \mathcal{P}_B^0$ (in dashed black) in the plots of $\mathcal{P}_B(k)$. We examine the spectrum and n_B over the range of scales where the spectrum rises towards the peak, and we inspect the behavior across a range of large negative values of $n_2 = [-20, -26]$ (on top panels). For this analysis we set the intermediate phase of J to be brief yet finite with $\Delta N_2 = 0.5$. We find that the spectral index $n_B \geq 5$ close to the peak. We also examine the spectrum and n_B across a range of $\Delta N_2 = [0, 0.5]$, setting $n_2 = -25$ (on bottom panels). Once again, n_B easily reaches values ≥ 5 for values of $\Delta N_2 \geq 0.4$.

the value of $n_2 = -3$ is the dual to the case of $n_2 = 2$ as they both lead to the same solution for \mathcal{A}_k when $\gamma = 0$. The choices of parameters are made to produce the peak in $\mathcal{P}_B(k)$ over small scales of around $k \simeq 10^{14} \text{ Mpc}^{-1}$ and hence induce gravitational waves over corresponding frequencies of $f \simeq 0.1 \text{ Hz}$. If this setup is realized in an ultra slow roll model suitable model of $J(\phi)$, N_1 denotes the onset of ultra slow roll regime and our choice is consistent with the corresponding constraint on it from observational data over large scales [40]. To understand the effect of these model parameters on $\mathcal{P}_B^\lambda(k)$, we vary them around the aforementioned fiducial values and examine the associated implications.

We begin by inspecting the behavior of $\mathcal{P}_B^\lambda(k)$ for each helicity against the variation of n_2 . In Fig. 2, we present the spectra $\mathcal{P}_B^{L,R}(k)$ computed numerically, and the total power spectrum $\mathcal{P}_B(k) = \mathcal{P}_B^L(k) + \mathcal{P}_B^R(k)$ across a range of choices for n_2 . The spectrum is scale-invariant and right-circular for $n_2 = 2$. As we vary $n_2 = [-3, 2]$, the features of dip, rise and peak become prominent in $\mathcal{P}_B^\lambda(k)$ of both helicities.

However, due to the parity-violating term in the action, the behavior around the peak are different for the two helicities. Although the overall power in right-circular mode is enhanced, and the left-circular mode suppressed – as expected with $\gamma \neq 0$ – the trend is *reversed* around the scales approaching the peak of the spectrum. This phenomenon leads to a double-peaked structure of total magnetic power, characterized by altering helicities. We interpret it as due to interplay of democratic enhancement in power in both helicities due to the intermediate phase of $J(N)$ and a preferential enhancement arising

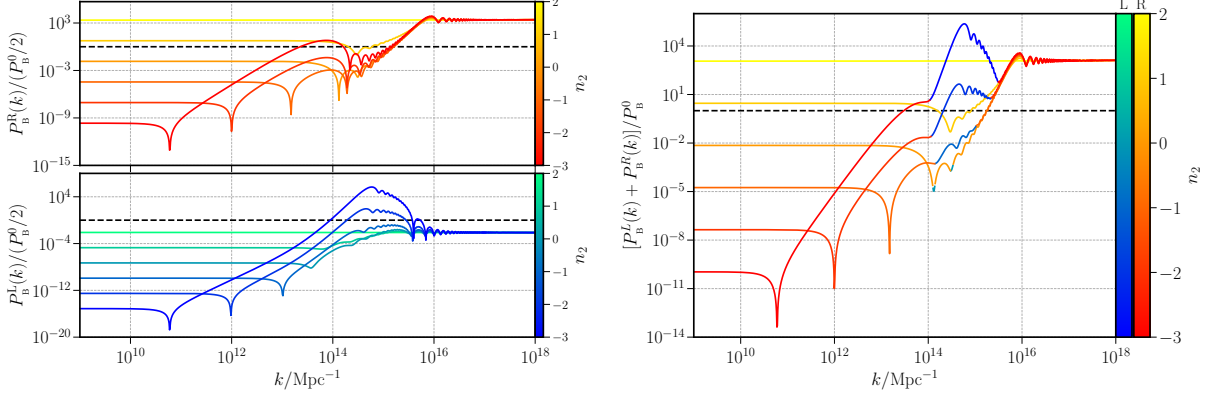


Figure 2: We present $\mathcal{P}_B^L(k)/(P_B^0/2)$ and $\mathcal{P}_B^R(k)/(P_B^0/2)$ (on the left) and the total power spectrum $\sum_\lambda \mathcal{P}_B^\lambda(k)/P_B^0$ (on the right) across a range of $n_2 = [-3, 2]$. For reference, we also plot the spectrum of the non-helical case without the intermediate phase of J where $\mathcal{P}_B^L = \mathcal{P}_B^R = P_B^0/2$ (in dashed black). We have chosen $\gamma = 1$, $N_1 = 15$ and $\Delta N_2 = 3$ in the functional form of $J(N)$. This choice of parameters lead to the wavenumber corresponding to the onset of the intermediate phase of J to be $k_1 = 9.92 \times 10^{13} \text{ Mpc}^{-1}$. For $n_2 = 2$, we obtain $\mathcal{P}_B^L(k)$ and $\mathcal{P}_B^R(k)$ to be scale-invariant but with a significant difference in magnitude due to non-zero γ . With the decrease in n_2 , the features of dip, rise and peak become prominent in both the spectra. The total power spectrum (on the right) is predominantly right-circular but for a brief window of scales between the asymptotic values, where the power increases and turns left-circular in polarization with decrease in n_2 . Hence, for $n_2 = -3$ with $\Delta N_2 = 3$, we obtain an interesting double-peaked spectrum with distinct polarization for each peak.

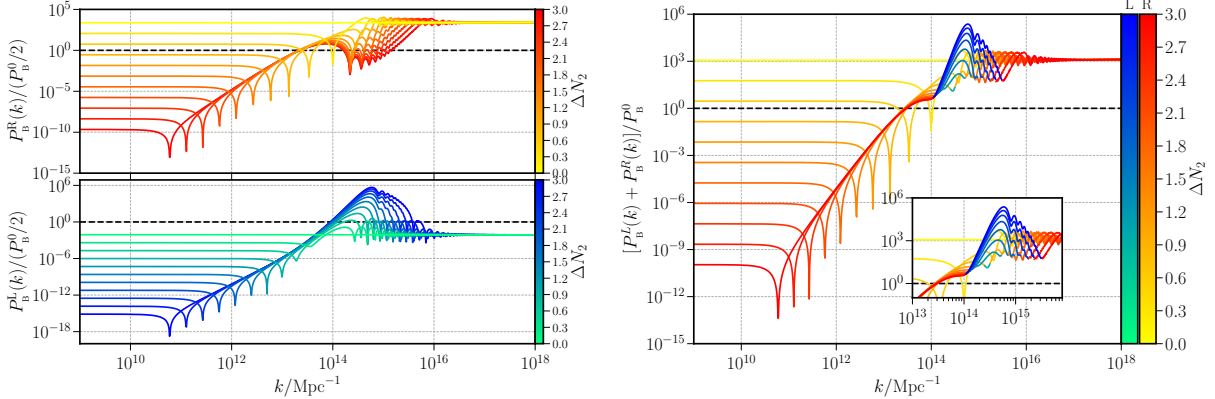


Figure 3: We present $\mathcal{P}_B^L(k)$ and $\mathcal{P}_B^R(k)$ (on the left) and the total power spectrum $\sum_\lambda \mathcal{P}_B^\lambda(k)$ (on the right) across a range of $\Delta N_2 = [0, 3]$, in terms of P_B^0 as in Fig. 2. We also plot the reference spectrum of $\mathcal{P}_B^L = \mathcal{P}_B^R = P_B^0/2$ (in dashed black). We have chosen $\gamma = 1$, $N_1 = 15$ and $n_2 = -3$ in the functional form of $J(N)$. For $\Delta N_2 = 0$, we obtain $\mathcal{P}_B^L(k)$ and $\mathcal{P}_B^R(k)$ to be scale-invariant but with $\mathcal{P}_B^R(k)$ dominating over $\mathcal{P}_B^L(k)$. With the increase in ΔN_2 , the features of dip, rise and peak become prominent in both the spectra. Around the peak of the spectra, $\mathcal{P}_B^L(k)$ begins to dominate over $\mathcal{P}_B^R(k)$ with increase in ΔN_2 . The total power spectrum (on the right) is predominantly right-circular but for the window of scales that is peaked and left-circular in polarization (as focussed in the inset).

from the parity-violating term. Since for values of $n_2 \neq 2$ the right-circular mode is suppressed with respect to the left-circular mode around the peak, the prominent peak of the power spectrum is left-circular in an otherwise right-circular spectrum. We shall inspect this feature more closely in the next Section 3.3. See also [41] for related results in a similar context.

We then inspect the effect of the duration of the intermediate phase ΔN_2 on the features $\mathcal{P}_B(k)$. We set $n_2 = -3$ and $\gamma = 1$, and present the results in Fig. 3. Once again, as we vary $\Delta N_2 = [0, 3]$, we find the features of dip, rise and peak becoming prominent in $\mathcal{P}_B^\lambda(k)$ for both helicities. Moreover, the altering

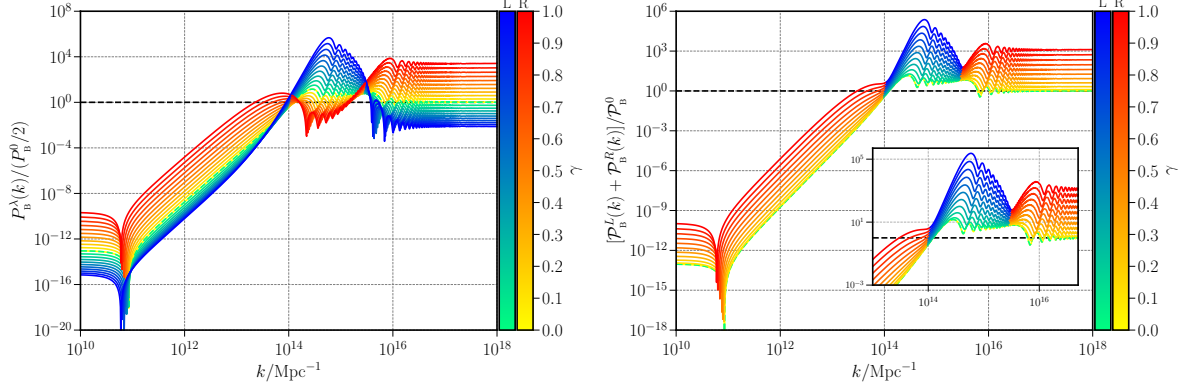


Figure 4: We present the magnetic power spectrum $\mathcal{P}_B^\lambda(k)$ for a range of $\gamma = [0, 1]$ for individual helicities (on the left) and for the sum of both helicities (on the right) in terms of \mathcal{P}_B^0 as in Figs. 2 and 3. The parameters of the model are set to be $N_1 = 15, n_2 = -3, \Delta N_2 = 3$. Evidently, for $\gamma = 0$, we have both left and right helical modes having the same spectra. The inset on the right panel zooms in on the range of scales around the peak that shall be relevant for the behavior of the spectra of induced GW. Note that the case of $\gamma = 1$ generates an amplification of about 10^5 compared to the non-helical case of $\gamma = 0$ at the peak of the spectrum.

helicity at the peak of the spectrum also becomes prominent with increase in ΔN_2 .

Lastly, we repeat our analysis varying the constant parameter γ within the interval $\gamma = [0, 1]$. We set $n_2 = -3$ and $\Delta N_2 = 3$ and present the spectra in Fig. 4. We observe that for $\gamma = 0$, $\mathcal{P}_B^L(k) = \mathcal{P}_B^R(k)$ with features of dip, rise and peak in the spectra, as described in [21]. For values of $\gamma > 0$, we notice an overall enhancement of $\mathcal{P}_B^R(k)$ and a suppression of $\mathcal{P}_B^L(k)$, except around the peak. Around the peak, in fact, we have a reversal of this trend, as noted earlier.

Besides, in the non-helical case of our setup ($\gamma = 0$), the spectrum of electric field at the end of inflation $\mathcal{P}_E^\lambda(k)$ behaves as $\mathcal{P}_E^\lambda(k) \simeq \mathcal{P}_B^\lambda(k)(k/k_e)^2$, with k_e corresponding to the wavenumber at the end of inflation. It turns out to be $\mathcal{P}_E^\lambda(k) \simeq \mathcal{P}_B^\lambda(k)$ when we turn on γ and becomes $\mathcal{P}_E^\lambda(k) = \mathcal{P}_B^\lambda(k)$ when $\gamma = 1$, consistently mimicking the features in the spectrum, including alteration of helicity. However, the electric field gets shorted during reheating with the production of charged particles and the associated high conductivity of the epoch [16, 28].

Regarding the bound on the magnetic field strength over CMB scales, we can see that our model consistently leads to $\mathcal{P}_B(k) \ll \mathcal{P}_B^0$ over large scales, compared to \mathcal{P}_B^0 over small scales. For the fiducial values of $n_2 = -3$ and $\Delta N_2 = 3$, with $\gamma = 0$, we obtain $\mathcal{P}_B(k) \simeq 10^{-13} \mathcal{P}_B^0$ over CMB scales. We have worked with Hubble parameter to be $H \simeq 7 \times 10^{-6} M_{Pl}$, consistent with the bound on tensor-to-scalar ratio from CMB anisotropies. This leads to the magnetic field strength today over scales larger than 1 Mpc to be about $B_{1\text{Mpc}} \simeq 10^{-15}$ G (for explicit calculations, see for instance [19, 20]). For $\gamma = 1$, we get $\mathcal{P}_B(k) \simeq 10^{-10} \mathcal{P}_B^0$ over CMB scales and hence $B_{1\text{Mpc}} \simeq 3 \times 10^{-14}$ G. These values are consistent with the existing lower bound on the parameter [42].

3.3 Altering helicities at the peak - an analytical understanding

The curious feature of altering helicities around the peak value of $\mathcal{P}_B(k)$ warrants closer examination and we may understand this effect in the following way. Recall that the equation of motion governing \mathcal{A}_k is Eq. (2.3)

$$\mathcal{A}_k^{\lambda''} + \left(k^2 + 2\xi^\lambda \gamma k \frac{J'}{J} - \frac{J''}{J} \right) \mathcal{A}_k^\lambda = 0. \quad (3.2)$$

During the phase when $J \propto a^2 \propto \tau^{-2}$ we get $J'/J = |2/\tau|$ and $J''/J = 6/\tau^2$. Hence, the equation becomes

$$\mathcal{A}_k^{\lambda''} + \left(k^2 + 4\xi^\lambda \gamma \left| \frac{k}{\tau} \right| - \frac{6}{\tau^2} \right) \mathcal{A}_k^\lambda = 0. \quad (3.3)$$

The parity-violating term enhances \mathcal{A}_k^R (with $\xi^R = -1$) and suppresses \mathcal{A}_k^L (with $\xi^L = 1$) for wavenumbers exiting the Hubble radius, i.e. $|k\tau| \simeq \sqrt{6}$ during this regime. The behavior of the enhanced mode in the asymptotic regime of $|k\tau| \ll 1$ is [25]

$$\mathcal{A}_k^R \propto \frac{e^{2\pi\gamma}}{(2\gamma)^{3/2}}. \quad (3.4)$$

On the other hand, in the phase when $J \propto a^{-3} \propto \tau^3$ we get $J'/J = -|3/\tau|$ while $J''/J = 6/\tau^2$. This leads to the equation of motion being

$$\mathcal{A}_k^{\lambda''} + \left(k^2 - 6\lambda\gamma \left| \frac{k}{\tau} \right| - \frac{6}{\tau^2} \right) \mathcal{A}_k^\lambda = 0. \quad (3.5)$$

The difference in sign of J'/J with respect to the earlier case leads to opposite effect on helicities. The parity-violating term now enhances \mathcal{A}_k^L and suppresses \mathcal{A}_k^R for modes attaining $|k\tau| \simeq \sqrt{6}$ during this regime. The behavior of the enhanced mode in the asymptotic regime of $|k\tau| \ll 1$ is

$$\mathcal{A}_k^L \propto \frac{e^{3\pi\gamma}}{(3\gamma)^{3/2}}. \quad (3.6)$$

Thus we have different helicities enhanced over wavenumbers exiting Hubble radius in different regimes of $J(\tau)$.

Note that the enhancement of the mode function exiting Hubble radius during the phase of $J \propto a^{-3}$ is larger by a factor of $3/2$ in the exponent compared to the mode function exiting in the phase of $J \propto a^2$, i.e.

$$\mathcal{A}_{k(J \sim a^{-3})}^L \propto \left[\mathcal{A}_{k(J \sim a^2)}^R \right]^{3/2}. \quad (3.7)$$

Hence the corresponding power spectra for the two cases may be related as

$$\mathcal{P}_{\text{B}}^L(k)_{(J \sim a^{-3})} \propto \left[\mathcal{P}_{\text{B}}^R(k)_{(J \sim a^2)} \right]^{3/2}. \quad (3.8)$$

This relation explains the difference between enhancements of amplitudes of power over large scales and the power at the peak. For $\gamma = 1$, over large scales $\mathcal{P}_{\text{B}}^L(k \ll k_1)$ is enhanced by about 10^3 compared to the case of $\gamma = 0$. The value $\mathcal{P}_{\text{B}}^R(k \simeq k_1)$ around the peak is enhanced by about $10^{9/2} \simeq 3 \times 10^5$.

3.4 Backreaction

The issue of backreaction may become crucial in the presence of parity-violating interactions, which lead to chiral instabilities [19, 29, 30, 43–45]. To trust our set-up, we must ensure that the energy density of the electromagnetic field ρ_{EM} remains sub-dominant to the background energy density driving inflation ρ_i . In case of magnetogenesis with monotonic evolution of the coupling function J , value of $\gamma \gtrsim 2.5$ is shown to cause strong backreaction [19]. Interestingly, we *do not encounter* issues with backreaction in our scenario, making it a viable model for chiral magnetogenesis from inflation without issues related with backreaction.

In fact, let us examine the case of a three-phase evolution of $J(N)$ in the scenario we are considering here. Recall that the tensor power spectrum $\mathcal{P}_{\text{T}}(k) \simeq 2H^2/M_{\text{Pl}}^2$. Therefore the background energy density during inflation is $\rho_i(\tau)$

$$\rho_i(\tau) = 3H^2 M_{\text{Pl}}^2 \simeq M_{\text{Pl}}^4 \mathcal{P}_{\text{T}}(k). \quad (3.9)$$

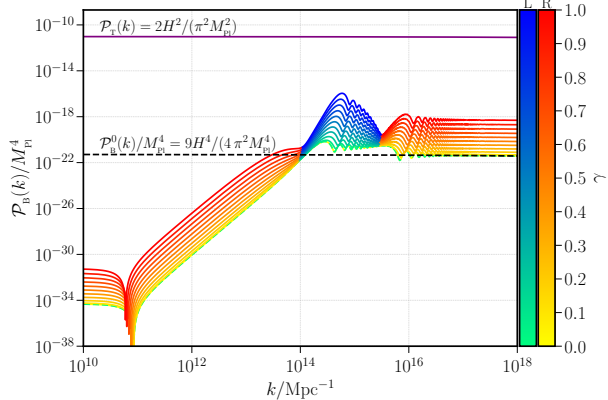


Figure 5: The total power spectrum $\mathcal{P}_B(k) = \sum_\lambda \mathcal{P}_B^\lambda$ is presented in units of M_{Pl}^4 against the power spectrum of primary tensor perturbations $\mathcal{P}_T(k)$, for a range of $\gamma = [0, 1]$. We set the model parameters to be $n_2 = -3$, $N_1 = 15$ and $\Delta N_2 = 3$. The plot illustrates that the ratio of $\mathcal{P}_B(k)/(\mathcal{P}_T(k)M_{Pl}^4)$ is small even at the peak amplitude of $\mathcal{P}_B(k)$. At the asymptotic value over small scales, this ratio is approximately $\mathcal{P}_B(k)/(\mathcal{P}_T(k)M_{Pl}^4) \simeq f(\gamma)(H/M_{Pl})^2$, where $f(\gamma)$ is typically $\mathcal{O}(10^3)$ for $\gamma = 1$. So, as long as $H/M_{Pl} \leq 10^{-3/2}$, the backreaction due to electromagnetic energy density is small in the model of interest.

On the other hand, the electromagnetic energy density is

$$\rho_{EM}(\tau) = \frac{1}{2} \int d \ln k [\mathcal{P}_B(k) + \mathcal{P}_E(k)] \simeq \int d \ln k \mathcal{P}_B(k), \quad (3.10)$$

where the last expression is justified in case of $\gamma = \mathcal{O}(1)$ leading to $\mathcal{P}_B(k) \simeq \mathcal{P}_E(k)$. Hence, $\mathcal{P}_B(k)/(\mathcal{P}_T(k)M_{Pl}^4)$ is an equivalent estimate of ρ_{EM}/ρ_1 . Ensuring this ratio to remain below unity across scales indicates control over backreaction.

We illustrate the comparison of $\mathcal{P}_B(k)$ against $M_{Pl}^4 \mathcal{P}_T(k)$ in Fig. 5 over the range of values of γ we work with. (We choose $H \simeq 7 \times 10^{-6} M_{Pl}$, so to be consistent with bounds on the tensor to scalar ratio over CMB scales.) The spectrum $\mathcal{P}_B(k)$ is suppressed from $\mathcal{P}_B^0 = 9H^4/4\pi^2$ over large scales, and so it is very small compared to $M_{Pl}^4 \mathcal{P}_T(k)$. Crucially, the ratio of $\mathcal{P}_B(k)/(\mathcal{P}_T(k)M_{Pl}^4)$ is small at the peak amplitude of $\mathcal{P}_B(k)$, even for the maximum value of $\gamma = 1$. Over small scales, where $\mathcal{P}_B(k)$ settles to the asymptotic value of \mathcal{P}_B^0 , this ratio becomes $\mathcal{P}_B(k)/(\mathcal{P}_T(k)M_{Pl}^4) \simeq f(\gamma)(H/M_{Pl})^2$, where $f(\gamma)$ is $\mathcal{O}(10^3)$ for $\gamma = 1$ [19, 29, 30]. So – as long as $H/M_{Pl} \leq 10^{-3/2}$ – thanks to the fact that the magnetic field is enhanced rapidly at small scales only, we conclude that the backreaction due to electromagnetic field is negligible, as stated above.

4 Second scenario: analytical results

In this section we present a second scenario for non-slow-roll magnetogenesis. We extend the analytical methods of [21] to a setup including parity violation, with the aim of obtaining analytic insight into the numerical results presented in Section 3. The approach closely follows the techniques of [22, 23], adapted to our context; differences and clarifications are discussed where relevant.

The starting point is the evolution equation for the helical modes during de Sitter inflation – Eq. (2.3) which we report here:

$$\mathcal{A}_k^\lambda''(\tau) + \left(k^2 + 2\lambda k \gamma(\tau) \frac{J'(\tau)}{J(\tau)} - \frac{J''(\tau)}{J(\tau)} \right) \mathcal{A}_k^\lambda(\tau) = 0, \quad (4.1)$$

with $\lambda = \pm 1$, and where we allow $\gamma(\tau)$ to be time dependent.

As a reference, in the standard case in which $J(\tau) \propto a^2(\tau)$ and $\gamma(\tau) = 0$ during inflation, with

$a(\tau) = -1/(H_I \tau)$, the solution connected to the Bunch-Davies vacuum is the well-known mode function

$$\mathcal{A}_k(\tau) = \frac{3 a^2(\tau) H_I^2}{\sqrt{2} k^{5/2}} e^{-ik\tau} \left(1 + ik\tau - \frac{k^2 \tau^2}{3} \right). \quad (4.2)$$

We are interested in a general class of models in which

$$J(\tau) = a^2(\tau) \sqrt{\omega(\tau)}, \quad (4.3)$$

with $\omega(\tau_R) = 1$ at the end of inflation. We assume the following time dependence for the functions J and γ :

$$\omega(\tau) = \begin{cases} \omega_0 & \text{for } \tau < \tau_1, \\ \text{continuous but rapidly varying} & \text{for } \tau_1 < \tau < \tau_2, \\ 1 & \text{for } \tau_2 < \tau < \tau_R, \end{cases} \quad (4.4)$$

$$\gamma(\tau) = \begin{cases} 0 & \text{for } \tau < \tau_1, \\ \text{continuous but rapidly varying} & \text{for } \tau_1 < \tau < \tau_2, \\ 0 & \text{for } \tau_2 < \tau < \tau_R. \end{cases} \quad (4.5)$$

The two times τ_1 and τ_2 are close to each other – in fact we assume

$$\frac{\tau_2 - \tau_1}{\tau_1} \ll 1, \quad (4.6)$$

so that the interval $\tau_1 < \tau < \tau_2$ is short: within this brief period $J(\tau)$ may significantly deviate from a power law and parity-violating effects encoded in $\gamma(\tau)$ can be active. (Later in this section, we consider the limit of Eq. (4.6) infinitesimally small.)

Physically, as described in the previous sections, this situation can be realised in inflationary models where the inflaton kinetic energy (or $\dot{\phi}$) changes rapidly for a short time. In such scenarios one can envisage set-up with $\gamma \sim \dot{\phi}^2$, so that γ is negligible during slow roll and becomes nonzero (and potentially large) only during the brief non-slow-roll phase. Notice that the choice of profile in Eq. (4.5) is different with respect to what discussed in Section 3.2, where we instead assume $\gamma = 1$ throughout inflation.

To obtain full analytic solutions for this system we adopt the following Ansatz for the mode function,

$$\begin{aligned} \mathcal{A}_k(\tau) = & \frac{3 a^2(\tau) \sqrt{\omega(\tau)} H_I^2}{\sqrt{2} k^{5/2}} e^{-ik\tau} \left[1 + ik\tau - \frac{k^2 \tau^2}{3} - k\tau_0 \Gamma_1(\tau) \right. \\ & \left. + (ik\tau_0)^2 (G_{(2)}(\tau) + i\Gamma_{(2)}(\tau)) + (ik\tau_0)^3 (G_{(3)}(\tau) + i\Gamma_{(3)}(\tau)) + \dots \right], \end{aligned} \quad (4.7)$$

where τ_0 is a pivot quantity whose explicit value will cancel out of final observables. The solution is constructed piecewise, extending the methods of [38]:

1. For $\tau < \tau_1$ we recover the standard solution ($J = a^2$, $\gamma = 0$) so all G_i, Γ_j vanish and we reduce to Eq. (4.2).
2. For $\tau_1 < \tau < \tau_2$ we determine the functions G_i, Γ_j by inserting the Ansatz (4.7) into Eq. (4.1) and solving order-by-order in powers of k .
3. For $\tau_2 < \tau < \tau_R$ we again have the standard slow-roll form ($J = a^2, \gamma = 0$) and we impose Israel matching conditions at $\tau = \tau_2$ to fix the post-intermediate-stage coefficients.

Working within the short interval $\tau_1 < \tau < \tau_2$, we expand all quantities about τ_1 and define $\Delta\tau \equiv \tau - \tau_1$ with $0 \leq \Delta\tau \ll \tau_1$. From the k^1 order we obtain the differential relation

$$\frac{d}{d\tau} \left[\frac{\tau_0 \omega(\tau) \Gamma_1'(\tau)}{\tau^4} \right] = \lambda \gamma(\tau) \frac{d}{d\tau} \left[\frac{\omega(\tau)}{\tau^4} \right], \quad (4.8)$$

which is formally integrated to

$$\tau_0 \Gamma_1(\tau) = \lambda \int_{-\infty}^{\tau} d\tau_a \frac{\tau_a^4}{\omega(\tau_a)} \int_{-\infty}^{\tau_a} d\tau_b \gamma(\tau_b) \frac{d}{d\tau_b} \left[\frac{\omega(\tau_b)}{\tau_b^4} \right]. \quad (4.9)$$

We introduce the following parameters evaluated at $\tau = \tau_1$,

$$\alpha \equiv \left(\frac{d \ln \omega}{d \ln \tau} \right)_{\tau=\tau_1}, \quad (4.10)$$

$$\beta \equiv \left(\frac{d \gamma}{d \ln \tau} \right)_{\tau=\tau_1}. \quad (4.11)$$

Expanding the formal solution (4.9) in $\Delta\tau$ we find that the leading nonzero contribution to Γ_1 is cubic,

$$\tau_0 \Gamma_1(\tau) = \lambda \frac{\beta(\alpha-4) \Delta\tau^3}{6\tau_1^2} + \mathcal{O}(\Delta\tau^4). \quad (4.12)$$

From the term k^2 in the expansion we obtain two conditions, which once Taylor-expanded in $\Delta\tau$ give

$$\tau_0^2 G_2(\tau) = \frac{\alpha}{6} \Delta\tau^2 + \mathcal{O}(\Delta\tau^3), \quad (4.13)$$

$$\tau_0^2 \Gamma_2(\tau) = \lambda \frac{\beta(\alpha-4)}{6\tau_1} \Delta\tau^3 + \mathcal{O}(\Delta\tau^4). \quad (4.14)$$

At k^3 order the leading results are

$$\tau_0^3 G_3(\tau) = \frac{\alpha}{6} \tau_1 \Delta\tau^2 + \mathcal{O}(\Delta\tau^3), \quad (4.15)$$

$$\tau_0^3 \Gamma_3(\tau) = \lambda \frac{\beta(\alpha-4)}{18} \Delta\tau^3 + \mathcal{O}(\Delta\tau^4). \quad (4.16)$$

For higher orders k^n with $n \geq 4$ the coefficients obey simple recursion relations (for derivatives evaluated at τ_1),

$$\tau_0^n G_n^{(n-1)}(\tau_1) = 2 \tau_0^{n-1} G_{n-1}^{(n-2)}(\tau_1), \quad (4.17)$$

$$\tau_0^n \Gamma_n^{(n)}(\tau_1) = 2 \tau_0^n \Gamma_{n-1}^{(n-1)}(\tau_1), \quad (4.18)$$

which imply

$$\tau_0^n G_n^{(n-1)}(\tau_1) = 2^{n-3} \frac{\alpha \tau_1}{3}, \quad (4.19)$$

$$\tau_0^n \Gamma_n^{(n)}(\tau_1) = 2^{n-3} \lambda \beta \frac{(\alpha-4)}{3}. \quad (4.20)$$

Hence, keeping leading Taylor terms for each $n \geq 3$,

$$\tau_0^n G_n(\tau) = 2^{n-3} \frac{\alpha \tau_1}{3} \frac{\Delta\tau^{n-1}}{(n-1)!} + \dots, \quad (4.21)$$

$$\tau_0^n \Gamma_n(\tau) = 2^{n-3} \lambda \beta \frac{(\alpha-4)}{3} \frac{\Delta\tau^n}{n!} + \dots \quad (4.22)$$

Plugging all these results in Ansatz (4.7), they lead to an exact resummation to exponentials. In fact, we use

$$\sum_{n=3}^{\infty} (ik\tau_0)^n G_{(n)}(\tau) = \frac{ik\tau_1 \alpha}{12} (e^{2ik\Delta\tau} - 1 - 2ik\Delta\tau), \quad (4.23)$$

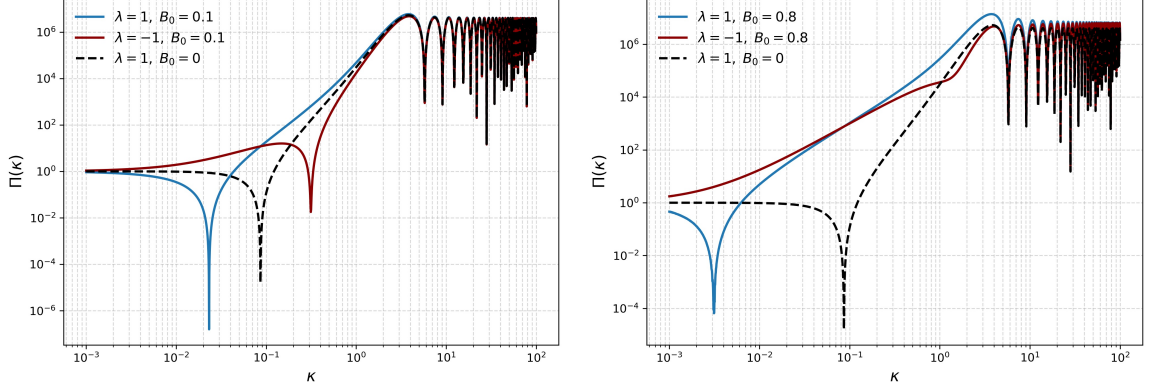


Figure 6: Analytical spectra evaluated with the limiting formula (4.32).

$$i \sum_{n=3}^{\infty} (ik\tau_0)^n \Gamma(n)(\tau) = i \lambda \beta \frac{(\alpha - 4)}{24} (e^{2ik\Delta\tau} - 1 - 2ik\Delta\tau + 2k^2\Delta\tau^2). \quad (4.24)$$

To conclude, the resulting mode function in the short interval $\tau_1 < \tau < \tau_2$ can be written as

$$\begin{aligned} \mathcal{A}_k(\tau) = & \frac{3a^2(\tau)\sqrt{\omega(\tau)}H_I^2}{\sqrt{2}k^{5/2}}e^{-ik\tau} \left[1 + ik\tau - \frac{k^2\tau^2}{3} - \lambda \frac{\beta(\alpha - 4)k\Delta\tau^3}{6\tau_1^2} \right. \\ & - k^2 \left(\frac{\alpha}{6}\Delta\tau^2 + i\lambda \frac{\beta(\alpha - 4)}{6\tau_1}\Delta\tau^3 \right) + \frac{ik\tau_1\alpha}{12}(e^{2ik\Delta\tau} - 1 - 2ik\Delta\tau) \\ & \left. + i\lambda\beta \frac{(\alpha - 4)}{24}(e^{2ik\Delta\tau} - 1 - 2ik\Delta\tau + 2k^2\Delta\tau^2) \right]. \end{aligned} \quad (4.25)$$

This expression displays the explicit chirality dependence through λ and captures the leading modifications arising from the short non-slow-roll episode.

Matching this intermediate solution to the final slow-roll phase using Israel junction conditions yields, for $\tau > \tau_2$, the standard form

$$\mathcal{A}_k(\tau) = \frac{3a^2(\tau)H_I^2}{\sqrt{2}k^{5/2}} \left[C_1 \left(1 + ik\tau - \frac{k^2\tau^2}{3} \right) e^{-ik\tau} + C_2 \left(1 - ik\tau - \frac{k^2\tau^2}{3} \right) e^{ik\tau} \right], \quad (4.26)$$

where the coefficients $C_{1,2}$ are fixed by the matching conditions of the function and its derivatives at τ_2 .

We proceed making additional steps that further simplify our expressions for the mode functions. We take the limits

$$\begin{aligned} \Delta\tau &\rightarrow 0, \quad \alpha \rightarrow \infty, \quad \beta \rightarrow \infty \\ \alpha\Delta\tau &= 2\Pi_0, \quad \Pi_0\beta/\alpha = B_0 \end{aligned} \quad (4.27)$$

keeping Π_0, B_0 finite. This is motivated by the 't Hooft limit [46] which one encounters in particle physics. We work in terms of the dimensionless quantity

$$\kappa = -k\tau_1 \quad (4.28)$$

with τ_1 the conformal time during inflation when the non-slow-roll phase occurs. Then, the quantities $C_{1,2}$ appearing in Eq. (4.26) reduce to

$$C_1 = 1 + \left(1 - \frac{3i}{\kappa^3} - \frac{2i}{\kappa} - \frac{iB_0(9 + 3\kappa^2 + \kappa^4)\lambda}{\kappa^4} \right) \Pi_0, \quad (4.29)$$

$$C_2 = -\frac{e^{2i\kappa}(i+\kappa)(-3+3i\kappa+\kappa^2)\Pi_0}{\kappa^3} + \frac{iB_0e^{2i\kappa}(-3+3i\kappa+\kappa^2)^2\lambda\Pi_0}{\kappa^4}. \quad (4.30)$$

These remarkably simple formulas, once plugged in Eq. (4.26), lead to a simple, exact expression for the parity violating vector mode function in the final epoch $\tau \geq \tau_2$ after the non-slow-roll phase occurs.

The amplitude of the resulting power spectrum at the end of inflation, normalized by its value at large scales, results

$$\Pi(\kappa) = \frac{\mathcal{P}_B(\kappa)}{\mathcal{P}_B(\kappa \rightarrow 0)} \quad (4.31)$$

$$= |C_1 + C_2|^2 \quad (4.32)$$

We plot it in Fig. 6 for a representative choice of parameters. Notice that also in this analytical Scenario 2 we find evidence for the phenomenon of ‘chirality flip’ towards the peak, as found in Section 3 for Scenario 1. More generally, for intermediate values of the parameter B_0 connected to the parity-violating effects, we notice that the profiles of the resulting chiral spectra resemble the numerical results of Section 3. We conclude that the analytical approach of this Section is able to capture the most important features of the system in terms of very simple, analytical expressions for the parity-violating mode functions.

5 Chiral gravitational waves from magnetic fields

Our results so far indicate that a short phase of non-slow-roll dynamics can considerably enhance the spectrum of primordial magnetic field at small scales. In this section we study the consequences of this phenomenon for the production of a chiral stochastic gravitational wave (GW) background induced at the second order by the chiral magnetic field.

The topic of vector induced GW has been developed in various works [47, 48], and the role of helical magnetic fields investigated in [25]. Our discussion aims to develop more systematic arguments and general formulas that can be used in our context of non-slow-roll magnetogenesis. We generalize the approach of [21] to study the generation of GW from the EM field during the radiation dominated epoch following inflation. Recall that the conformal invariance of the EM field is restored post inflation, since $J = 1$ at the end of inflation. The Fourier decomposition of the electromagnetic vector potential is

$$A_i(\tau, \mathbf{x}) = \sum_{\lambda=L}^R \int \frac{d^3\mathbf{k}}{(2\pi)^3} e^{i\mathbf{k}\cdot\mathbf{x}} e_i^{(\lambda)}(\hat{k}) A_\lambda(\tau, \mathbf{k}), \quad (5.1)$$

where $e_i^{(\lambda)}(\hat{k})$ are two orthonormal polarization vectors satisfying $e_i^{(\lambda)}\hat{k}_i = 0$. Vectors with a hat denote unit vectors, $\hat{k} = \mathbf{k}/k$ with $k \equiv |\mathbf{k}|$. The helicity polarization vectors obey the eigenrelation

$$(i\varepsilon_{ijk}k_j) e_l^{(\lambda)}(\hat{k}) = \xi^\lambda k e_i^{(\lambda)}(\hat{k}), \quad \xi^L = -\xi^R = 1, \quad (5.2)$$

and the normalization $e_i^{(\lambda)}e_i^{(\sigma)*} = \delta^{\lambda\sigma}$. The comoving magnetic field is defined by

$$B_i(\tau, \mathbf{x}) = \varepsilon_{ijk}\partial_j A_k(\tau, \mathbf{x}), \quad B_i(\tau, \mathbf{k}) = i\varepsilon_{ijk}k_j A_l(\tau, \mathbf{k}). \quad (5.3)$$

Using (5.2) and the expansion (5.1) we obtain

$$B_i(\tau, \mathbf{k}) = \sum_{\lambda=L,R} \xi^\lambda k e_i^{(\lambda)}(\hat{k}) A_\lambda(\tau, \mathbf{k}). \quad (5.4)$$

We assume the two helicities of the vector potential have (in general) different spectra:

$$\langle A_\lambda(\tau, \mathbf{k}) A_\sigma^*(\tau, \mathbf{q}) \rangle' = \delta_{\lambda\sigma} \frac{2\pi^2}{k^3} \mathcal{P}_A^\lambda(k), \quad (5.5)$$

where the prime over the expectation value denotes the quantity barring the associated Dirac delta function, here $\delta^{(3)}(\mathbf{k} - \mathbf{q})$. We define symmetric and helical combinations of $\mathcal{P}_A(k)$ as

$$\mathcal{P}_A^S(k) \equiv \frac{\mathcal{P}_A^L(k) + \mathcal{P}_A^R(k)}{2}, \quad \mathcal{P}_A^H(k) \equiv \frac{\mathcal{P}_A^L(k) - \mathcal{P}_A^R(k)}{2}. \quad (5.6)$$

The quantity $\mathcal{P}_A^H(k)$ controls the amount of helicity in the vector sector. It is controlled by the quantity γ in the specific scenarios discussed in Sections 3 and 4. With these ingredients we can compute the magnetic-field two-point functions:

$$\begin{aligned} \langle B_i(\mathbf{k}) B_j^*(\mathbf{q}) \rangle' &= \sum_{\lambda, \sigma} \xi^\lambda \xi^\sigma k^2 e_i^{(\lambda)}(\hat{k}) e_j^{(\sigma)*}(\hat{k}) \langle A_\lambda(\mathbf{k}) A_\sigma^*(\mathbf{q}) \rangle' \\ &= \sum_{\lambda} (\xi^\lambda)^2 k^2 e_i^{(\lambda)}(\hat{k}) e_j^{(\lambda)*}(\hat{k}) \frac{2\pi^2}{k^3} \mathcal{P}_A^\lambda(k) \\ &= \frac{2\pi^2}{k} \sum_{\lambda=L,R} \mathcal{P}_A^\lambda(k) e_i^{(\lambda)}(\hat{k}) e_j^{(\lambda)*}(\hat{k}). \end{aligned} \quad (5.7)$$

We now make use of the helicity-basis identity

$$e_i^{(\lambda)}(\hat{k}) e_j^{(\lambda)*}(\hat{k}) = \frac{1}{2} \left(\pi_{ij}(\hat{k}) + i \xi^\lambda \varepsilon_{ijl} \hat{k}_l \right), \quad (5.8)$$

to obtain

$$\begin{aligned} \langle B_i(\mathbf{k}) B_j^*(\mathbf{q}) \rangle' &= \frac{2\pi^2}{k} \frac{1}{2} \left[\pi_{ij}(\hat{k}) (\mathcal{P}_A^L(k) + \mathcal{P}_A^R(k)) + i \varepsilon_{ijl} \hat{k}_l (\mathcal{P}_A^L(k) - \mathcal{P}_A^R(k)) \right] \\ &= \frac{2\pi^2}{k} \left[\pi_{ij}(\hat{k}) \mathcal{P}_A^S(k) + i \varepsilon_{ijl} \hat{k}_l \mathcal{P}_A^H(k) \right]. \end{aligned} \quad (5.9)$$

This is the usual decomposition into parity-even (symmetric) and parity-odd parts: note the explicit factor i in front of the Levi-Civita tensor for the parity-odd contribution (this is required for the correlator to have the correct Hermiticity properties).

In order to map to the more common k^{-3} convention for the magnetic field spectrum, we define the associated magnetic spectra by

$$\mathcal{P}_B^S(k) \equiv k^2 \mathcal{P}_A^S(k), \quad \mathcal{P}_B^H(k) \equiv k^2 \mathcal{P}_A^H(k). \quad (5.10)$$

Then

$$\langle B_i(\mathbf{k}) B_j^*(\mathbf{q}) \rangle' = \frac{2\pi^2}{k^3} \left[\pi_{ij}(\hat{k}) \mathcal{P}_B^S(k) + i \varepsilon_{ijl} \hat{k}_l \mathcal{P}_B^H(k) \right]. \quad (5.11)$$

We now proceed computing the GW spectrum induced at second order by the enhanced magnetic field configuration. After the end of inflation, tensor perturbations h_{ij} obey

$$h_{ij}''(\tau, \mathbf{x}) + 2\mathcal{H}(\tau) h_{ij}'(\tau, \mathbf{x}) - \nabla^2 h_{ij}(\tau, \mathbf{x}) = \Pi_{ij}^{(T)}(\tau, \mathbf{x}), \quad (5.12)$$

where $\Pi_{ij}^{(T)}$ is the transverse-traceless (TT) part of the anisotropic stress associated with the amplified magnetic field. In Fourier space we decompose

$$h_{ij}(\tau, \mathbf{x}) = \sum_{\lambda=\pm 2} \int \frac{d^3 \mathbf{k}}{(2\pi)^3} e^{i\mathbf{k}\cdot\mathbf{x}} e_{ij}^{(\lambda)}(\mathbf{k}) h_{\mathbf{k}}^{(\lambda)}(\tau), \quad (5.13)$$

where the spin-2 polarization tensors $e_{ij}^{(\lambda)}(\mathbf{k})$ with $\lambda = [L, R] = \pm 2$, are given by the product of two spin-1 tensors used to decompose the vector fields in Eq. (5.1): $e_{ij}^{(\lambda)} = e_i^{(\lambda)} e_j^{(\lambda)}$. The evolution equation for each Fourier mode for the spin-2 GW is

$$h_{\mathbf{k}}^{(\lambda)''} + 2\mathcal{H} h_{\mathbf{k}}^{(\lambda)'} + k^2 h_{\mathbf{k}}^{(\lambda)} = S^{(\lambda)}(\tau, \mathbf{k}), \quad (5.14)$$

where the source term is the TT-projection of the magnetic stress:

$$\begin{aligned} S^{(\lambda)}(\tau, \mathbf{k}) &\equiv e^{(\lambda)ij}(\hat{k}) \Pi_{ij}^{(T)}(\tau, \mathbf{k}) = \frac{e^{(\lambda)ij}(\hat{k}) \Lambda_{ij}^{mn} \tau_{mn}^B(\mathbf{k})}{a^2(\tau)}, \\ &= \frac{e^{(\lambda)ij}(\hat{k}) \tau_{ij}^B(\mathbf{k})}{a^2(\tau)}. \end{aligned} \quad (5.15)$$

To write these equalities we used the definition of projector Λ :

$$\Lambda_{ij}^{\ell m} = \frac{1}{2} \sum_{\lambda} e_{ij}^{(\lambda)} e^{(\lambda)\ell m} = \frac{1}{2} (\pi_i^{\ell} \pi_j^m + \pi_j^{\ell} \pi_i^m - \pi_{ij} \pi^{\ell m}), \quad \pi_{ij} = \delta_{ij} - \hat{k}_i \hat{k}_j, \quad (5.16)$$

The magnetic stress tensor is

$$\tau_{ij}^{(B)}(\mathbf{k}) = \frac{1}{4\pi} \int \frac{d^3 p}{(2\pi)^3} \left[B_i(\mathbf{p}) B_j(\mathbf{k} - \mathbf{p}) - \frac{\delta_{ij}}{2} B_m(\mathbf{p}) B_m(\mathbf{k} - \mathbf{p}) \right]. \quad (5.17)$$

We ignore the contribution from electric field in the source as it gets shorted during reheating, as mentioned earlier. The formal solution of Eq. (5.14) is

$$h_{\mathbf{k}}^{(\lambda)}(\tau) = \frac{1}{a(\tau)} \int d\tau' g_k(\tau, \tau') a(\tau') S_{\mathbf{k}}^{(\lambda)}(\tau'), \quad (5.18)$$

where $g_k(\tau, \tau')$ is the Green function. During radiation domination the Green function is

$$g_k(\tau, \tau') = \frac{1}{k} [\sin(k\tau) \cos(k\tau') - \sin(k\tau') \cos(k\tau)]. \quad (5.19)$$

The two point function (rescaled towards the standard power-spectrum definition) reads

$$\begin{aligned} \frac{1}{2} \frac{k^3}{2\pi^2} \langle h_{\mathbf{k}}^{(\lambda)}(\tau) h_{\mathbf{q}}^{(\sigma)*}(\tau) \rangle'_{\mathbf{k}=\mathbf{q}} &= \frac{k^3}{4\pi^2 a^2(\tau)} \int d\tau_1 d\tau_2 g_k(\tau, \tau_1) g_k(\tau, \tau_2) a(\tau_1) a(\tau_2) \\ &\times \langle S_{\mathbf{k}}^{(\lambda)}(\tau_1) S_{\mathbf{k}}^{(\sigma)*}(\tau_2) \rangle'. \end{aligned} \quad (5.20)$$

We decompose GW correlators in terms of Stokes-like structures, focussing on intensity and circular polarization. Ignoring linear (spin-4) polarizations, the product of polarization tensors can be organized into parity-even and parity-odd parts as

$$e_{ij}^{(\lambda)} e_{mn}^{(\sigma)*} = \frac{\delta^{\lambda\sigma}}{2} \Lambda_{ijmn} + i \frac{\varepsilon^{\lambda\sigma}}{2} \Sigma_{ijmn}, \quad (5.21)$$

where Λ_{ijmn} is the symmetric TT combination (given in (5.16)) and $\varepsilon^{\lambda\sigma}$ the Levi-Civita tensor in two dimensions with $\varepsilon^{LR} = +1$. We conveniently define

$$X_{ij}(\hat{v}) \equiv \varepsilon_{ijl} \hat{v}_l, \quad (5.22)$$

and express Σ in the decomposition (5.21) as

$$\Sigma_{ijml}(\hat{k}) = \frac{1}{2} (\pi_{im}(\hat{k}) X_{jl}(\hat{k}) + \pi_{jl}(\hat{k}) X_{im}(\hat{k})). \quad (5.23)$$

We now collect these definitions and compute the source two-point function. We have

$$\begin{aligned} \langle S_{\mathbf{k}}^{(\lambda)}(\tau_1) S_{\mathbf{k}}^{(\sigma)*}(\tau_2) \rangle' &= \frac{e_{ij}^{(\lambda)} e_{mn}^{(\sigma)*}}{a^2(\tau_1) a^2(\tau_2)} \frac{(2\pi^2)^2}{(4\pi)^2} \int \frac{d^3 p}{(2\pi)^3 p^3 q^3} \times \\ &\times \left[(\pi_{im}(\hat{p}) \mathcal{P}_B^S(p) + i\Phi_{im}(\hat{p}) \mathcal{P}_B^H(p)) (\pi_{jn}(\hat{q}) \mathcal{P}_B^S(q) + i\Phi_{jn}(\hat{q}) \mathcal{P}_B^H(q)) \right. \end{aligned}$$

$$+ (m \leftrightarrow q) \Big] \quad (5.24)$$

with $\mathbf{q} = \mathbf{k} - \mathbf{p}$. We decompose $d^3p = 2\pi p^2 dp d\mu$, with $\mu = \mathbf{p} \cdot \mathbf{k}/(pk)$. We can write

$$\langle S_{\mathbf{k}}^{(\lambda)}(\tau_1) S_{\mathbf{k}}^{(\sigma)*}(\tau_2) \rangle' = \frac{k^{-3}}{4a^2(\tau_1)a^2(\tau_2)} \left[\delta^{\lambda\sigma} \Gamma_{\text{even}}(k) - \varepsilon^{\lambda\sigma} \Gamma_{\text{odd}}(k) \right], \quad (5.25)$$

where the scalar functions Γ_{even} (parity-even) and Γ_{odd} (parity-odd) are real. Taking into account of the properties of the Levi-Civita tensor, they are obtained by expanding Eq. (5.24), keeping the non-vanishing contributions:

$$\begin{aligned} \Gamma_{\text{even}}(k) = & \int \frac{dp d\mu}{p |\mathbf{q}|^3/k^3} \left\{ \Lambda_{ijmn}(\hat{k}) [\pi_{im}(p)\pi_{jn}(q) + \pi_{in}(p)\pi_{jm}(q)] \mathcal{P}_B^S(p) \mathcal{P}_B^S(q) \right. \\ & \left. - \Lambda_{ijmn}(\hat{k}) [\Phi_{im}(p)\Phi_{jn}(q) + \Phi_{in}(p)\Phi_{jm}(q)] \mathcal{P}_B^H(p) \mathcal{P}_B^H(q) \right\} \end{aligned} \quad (5.26)$$

and

$$\begin{aligned} \Gamma_{\text{odd}}(k) = & \int \frac{dp d\mu}{p |\mathbf{q}|^3/k^3} \left\{ \Sigma_{ijmn}(\hat{k}) [\pi_{im}(p)\Phi_{jn}(q) + \pi_{in}(p)\Phi_{jm}(q)] \mathcal{P}_B^S(p) \mathcal{P}_B^H(q) \right. \\ & \left. + \Lambda_{ijmn}(\hat{k}) [\Phi_{im}(p)\pi_{jn}(q) + \Phi_{in}(p)\pi_{jm}(q)] \mathcal{P}_B^H(p) \mathcal{P}_B^S(q) \right\} \end{aligned} \quad (5.27)$$

Using the dimensionless variables

$$u = \frac{|\mathbf{k} - \mathbf{p}|}{k}, \quad v = \frac{p}{k}, \quad \mu = \frac{\mathbf{k} \cdot \mathbf{p}}{kp} = \frac{1 - u^2 + v^2}{2v}, \quad (5.28)$$

we obtain the final convolution integrals

$$\begin{aligned} \Gamma_{\text{even}}(k; \tau_1, \tau_2) = & \int_0^\infty dv \int_{-1}^1 d\mu \frac{1}{u^3 v} \left[\mathcal{C}_{SS}(u, v, \mu) \mathcal{P}_B^S(ku) \mathcal{P}_B^S(kv) \right. \\ & \left. + \mathcal{C}_{HH}(u, v, \mu) \mathcal{P}_B^H(ku) \mathcal{P}_B^H(kv) \right], \end{aligned} \quad (5.29)$$

and

$$\begin{aligned} \Gamma_{\text{odd}}(k; \tau_1, \tau_2) = & \int_0^\infty dv \int_{-1}^1 d\mu \frac{1}{u^3 v} \\ & \times \left[\mathcal{C}_{\text{mix}}^A(u, v, \mu) \mathcal{P}_B^S(ku) \mathcal{P}_B^H(kv) + \mathcal{C}_{\text{mix}}^B(u, v, \mu) \mathcal{P}_B^H(ku) \mathcal{P}_B^S(kv) \right]. \end{aligned} \quad (5.30)$$

Here $\mathcal{C}_{SS}, \mathcal{C}_{HH}, \mathcal{C}_{\text{mix}}^{A,B}$ are scalar kernels obtained after contracting the geometric tensors with the TT projector and polarization tensors. After performing the necessary contractions the scalar kernels result

$$\mathcal{C}_{SS}(u, v, \mu) = \frac{(1 + \mu^2)(2 + v(v - 4\mu + v\mu^2))}{2(1 + v^2 - 2v\mu)} \quad , \quad \mathcal{C}_{HH}(u, v, \mu) = \frac{2\mu(-1 + v\mu)}{\sqrt{1 + v^2 - 2v\mu}} \quad (5.31)$$

$$\mathcal{C}_{\text{mix}}^A(u, v, \mu) = \frac{(1 - v\mu)(1 + \mu^2)}{\sqrt{1 + v^2 - 2v\mu}} \quad , \quad \mathcal{C}_{\text{mix}}^B(u, v, \mu) = \frac{\mu(2 + v(v - 4\mu + v\mu^2))}{1 + v^2 - 2v\mu} \quad (5.32)$$

Plugging these formulas into (5.20), the tensor two-point function can be compactly written as (a prime indicates correlators without the Dirac delta functions associated with momentum conservation)

$$\frac{1}{2} \frac{k^3}{2\pi^2} \langle h_{\mathbf{k}}^{(\lambda)}(\tau) h_{\mathbf{s}}^{(\sigma)*}(\tau) \rangle'_{\mathbf{k}=\mathbf{q}} = \frac{\pi}{2a^2(\tau)} \mathcal{I}_\tau^2 \mathcal{I}_{uv}^{(\lambda\sigma)}, \quad (5.33)$$

with

$$\mathcal{I}_\tau^2 = \left[\int_{\tau_R}^\tau \frac{d\tau_1}{a(\tau_1)} g_k(\tau, \tau_1) \right]^2, \quad (5.34)$$

$$\mathcal{I}_{uv}^{(\lambda\sigma)} = \delta^{\lambda\sigma} \Gamma_{\text{even}}(k; \tau_1, \tau_2) + \varepsilon^{\lambda\sigma} \Gamma_{\text{odd}}(k; \tau_1, \tau_2). \quad (5.35)$$

Notice that for vector-induced gravitational-wave spectra, the two-point correlator (5.33) factorizes into a product of a time integral and a momentum integral: the former depends only on Green's functions during radiation domination, while the latter encodes the properties of the magnetic-field source, see [21]. This separation allows us to estimate the two contributions independently.

Time integral: During radiation domination, $a(\tau)/a(\tau_1) = \tau/\tau_1$ and $a(\tau)H(\tau) = 1/\tau$. Averaging over rapid oscillations yields

$$\overline{\mathcal{I}_\tau^2} = \frac{1}{2k^2 a^4 H^2} \left[\text{Ci}(-k\tau_R)^2 + \left(\frac{\pi}{2} - \text{Si}(-k\tau_R) \right)^2 \right], \quad (5.36)$$

where Ci and Si are the cosine and sine integral functions. τ_R is a fiducial conformal time when the radiation domination epoch starts.

Momentum integral: We introduce the standard variables t and s via

$$u = \frac{t+s+1}{2}, \quad v = \frac{t-s+1}{2}. \quad (5.37)$$

Including the Jacobian for this transformation, we can carry out the momentum integral for $0 \leq t \leq \infty$ and $-1 \leq s \leq 1$.¹ The resulting GW energy density is (for the moment we keep the polarization indexes, later we define more ‘physical’ quantities)

$$\Omega_{\text{GW}}^{(\lambda\sigma)} = \frac{k^2}{12a^2 H^2} \times \frac{1}{2} \frac{k^3}{2\pi^2} \langle h_{\mathbf{k}}^{(\lambda)}(\tau) h_{\mathbf{q}}^{(\sigma)*}(\tau) \rangle' = \frac{\pi k^2}{24 a^4 H^2} \overline{\mathcal{I}_\tau^2} \mathcal{I}_{uv}^{(\lambda\sigma)}. \quad (5.38)$$

During radiation domination,

$$a(\tau) = H_0 \sqrt{\Omega_{\text{rd}}} \tau, \quad (5.39)$$

where H_0 and Ω_{rd} are the present-day Hubble parameter and radiation energy fraction. Defining $\hat{\Omega}_B = \rho_B/\rho_{\text{cr}} = \mathcal{P}_B^{\text{CMB}}/(3H_0^2)$ and including the redshift factor Ω_{rd} [49], we obtain

$$\Omega_{\text{GW}}^{(\lambda\sigma)}(\kappa) = \left[\frac{3\hat{\Omega}_B^2}{64\Omega_{\text{rd}}} \right] \left[\text{Ci}^2(\kappa x_\star) + \left(\frac{\pi}{2} - \text{Si}(\kappa x_\star) \right)^2 \right] \mathcal{I}_{uv}^{(\lambda\sigma)}(\kappa), \quad (5.40)$$

with $\kappa = -k\tau_1$, with $|\tau_1|$ the epoch during inflation associated with the non-slow-roll phase. The small parameter $x_\star = |\tau_R/\tau_1|$ controls the ratio between the relevant conformal times when radiation domination starts versus the non-slow-roll epoch, and enters only logarithmically in the final result; we adopt $x_\star = 10^{-4}$ for definiteness. The prefactor $[3\hat{\Omega}_B^2/64\Omega_{\text{rd}}]$ is fixed to be 2×10^{-48} as per the arguments presented in [21].

We can now introduce more physically-transparent combinations, by extracting the parity even and the parity odd parts of the GW spectrum, defined as

$$\Omega_{\text{GW}} = \Omega_{\text{GW}}^{(LL)} + \Omega_{\text{GW}}^{(RR)} \quad (5.41)$$

$$\Omega_{\text{GW}}^V = \Omega_{\text{GW}}^{(LL)} - \Omega_{\text{GW}}^{(RR)} \quad (5.42)$$

The quantity Ω_{GW} is the traditional GW energy density computed through the GW intensity, while Ω_{GW}^V aims at characterizing the effects of helical magnetic fields which induce circular polarization in the GW background.

¹For numerical implementation, we take the range of t to be $[10^{-2}, 200]$.

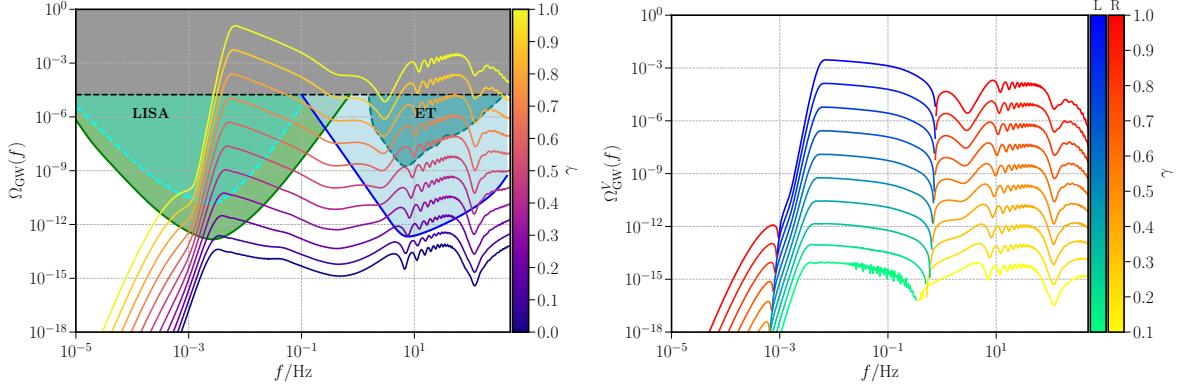


Figure 7: The spectral density Ω_{GW} and the associated V mode Ω_{GW}^V are presented for a range of $\gamma = [0, 1]$, corresponding to the magnetic spectra presented in Fig. 4. For reference, we plot the sensitivity curves of LISA (the nominal form in cyan and for the broken-power law case in green) and ET (the nominal form in teal and for the power-law case in blue) [50, 51]. We also demarcate the bound of $\Omega_{\text{GW}} < 1.74 \times 10^{-5}$ from BBN (in black dashed line) [52]. Beyond the overall amplification of Ω_{GW} due to non-zero γ , we find the spectrum having significant helicity as evidenced in Ω_{GW}^V . The feature of altering helicity of $\mathcal{P}_B(k)$ induces corresponding feature of altering chirality around the peak of GW spectra as seen in Ω_{GW}^V .

5.1 Results and implications for GW experiments

We compute the GW density parameter Ω_{GW} and associated chirality Ω_{GW}^V induced by the spectra $\mathcal{P}_B(k)$ using Eq. (5.40). We focus on our first scenario described in Section 3 – see the plot in Fig. 4. The behavior of the resulting GW spectra are illustrated in Fig. 7, where we plot Ω_{GW} and Ω_{GW}^V as functions of frequency. We set $n_2 = -3$, $\Delta N_2 = 3$ and the onset of the intermediate phase in J at $N_1 = 15$ such that the corresponding wavenumber $k_1 \simeq 10^{14} \text{ Mpc}^{-1}$. These choices are motivated by the requirement that the peak of Ω_{GW} enters in the range of interest for future GW experiments, once the units are converted into frequency expressed in Hertz (more on this later).

A parity-violating term in the action, controlled by the parameter γ , significantly increases the induction of GW. See Fig. 7, left panel. For example, choosing $\gamma = 1$ leads to an amplification of about 10^{12} in the amplitude of Ω_{GW} , when compared to $\gamma = 0$. This behaviour can be understood from the relation $\Omega_{\text{GW}} \propto \mathcal{P}_B^2$ and the amplification is about 10^6 at the peak of \mathcal{P}_B [cf. Fig. 4]. The bound from BBN already rules out a range of values of $\gamma > 0.7$ for the case of $n_2 = -3$ and $\Delta N_2 = 3$. As to $\Omega_{\text{GW}}(f)$, we find that the values of $\gamma \in [0.2, 0.7]$ leads to amplitude significant enough to be detected by the sensitivity of LISA. Besides, the features of the magnetic field spectral growth, its prominent peak, a second sub-dominant peak, and its subsequent oscillations as seen in $\mathcal{P}_B(k)$ are well reflected and captured in the $\Omega_{\text{GW}}(f)$ profile.

Turning to the behavior of chirality in the GW spectrum $\Omega_{\text{GW}}^V(f)$, the signature of altering helicities around the peak of $\mathcal{P}_B(k)$ is reproduced in the chirality of induced GW. See Fig. 7, right panel. Note that it is non-trivial to expect this behavior *a priori*, due to the non-linearities in the convolution integrals, and the specific integral kernels. We may see from the structure of the kernels involved in integration of source functions [cf. Eqs. (5.29) and (5.30)] that both polarizations of $\mathcal{P}_B^\lambda(k)$ contribute to both chiralities of $\Omega_{\text{GW}}^V(f)$. Nonetheless, we find that the peak amplitude of Ω_{GW}^V is positive (left-chiral) and it switches to negative values (right-chiral) on either sides. Moreover, we should note that for any given value of γ , the spectrum is never maximally chiral, i.e. $\Omega_{\text{GW}}^V/\Omega_{\text{GW}} < 1$. The reason being again that both polarizations of $\mathcal{P}_B^{\text{L},\text{R}}(k)$ contribute to a given chirality of induced GW.

Our findings open up interesting opportunities for GW experiments. It is well known that directly measuring GW circular polarization is challenging with planar detectors such as LISA [53, 54] and the Einstein Telescope (ET) [55], see e.g. [56] (as well as with pulsar timing arrays (see, e.g., [57])). Nevertheless, the two panels in Fig. 7 suggest at least two distinct strategies for detecting effects of parity violation in

the GW spectrum:

1. Information about chirality can be extracted from measurements of Ω_{GW} with LISA and ET in synergy [51]. In particular, as shown in the left panel of Fig. 7, Ω_{GW} exhibits a characteristic double-peak structure that would be accessible through a multiband detection with LISA and ET. Distinctive features of the second peak in the ET frequency band—such as the abrupt change in slope preceding the peak and the subsequent oscillatory behavior—depend sensitively on the value of the chirality parameter γ . Accurate measurements of the spectral shape of Ω_{GW} could therefore allow one to infer γ , potentially extending the reconstruction techniques developed in [58, 59].
2. For suitable choices of parameters, the amplitude of Ω_{GW}^V can be quite large, and at the same time Ω_{GW} satisfies BBN bounds at frequencies between the milli-Hertz and the tens of Hertz. Although Ω_{GW}^V can not be detected with measurements of the isotropic background, it can be measured from the properties of the kinematic dipole anisotropy [57, 60–63], which might be detectable in this regime.

A detailed quantitative investigation of both these possibilities is left for future work. Further, we must note that there are very few models of parity-violation that are known to generate strong signal of Ω_{GW} over a wide range of frequency with distinctly different chiralities of GW over different windows of frequencies (see [64, 65] for such scenarios). The narrow set of candidate models predicting altering chirality shall help in breaking of degeneracy during comparison against observations.

Acknowledgments

HVR acknowledges support by the MUR PRIN2022 Project “BROWSEPOL: Beyond standaRd mOdel With coSmic microwavE background POLarization”-2022EJNZ53 financed by the European Union - Next Generation EU. HVR acknowledges the use of computing cluster under University of Padova Strategic Research Infrastructure Grant 2017: “CAPRI: Calcolo ad Alte Prestazioni per la Ricerca e l’Innovazione”. GT is partially funded by the STFC grants ST/T000813/1 and ST/X000648/1. LS wishes to thank the Indo-French Centre for the Promotion of Advanced Research (IFCPAR/CEFIPRA), New Delhi, India, for support of the proposal 6704-4 titled ‘Testing flavors of the early universe beyond vanilla models with cosmological observations’ under the Collaborative Scientific Research Programme.

References

- [1] A. Maleknejad, M. M. Sheikh-Jabbari, and J. Soda, “Gauge Fields and Inflation,” *Phys. Rept.* **528** (2013) 161–261, [arXiv:1212.2921 \[hep-th\]](https://arxiv.org/abs/1212.2921).
- [2] M. S. Turner and L. M. Widrow, “Inflation Produced, Large Scale Magnetic Fields,” *Phys. Rev. D* **37** (1988) 2743.
- [3] B. Ratra, “Cosmological ‘seed’ magnetic field from inflation,” *Astrophys. J. Lett.* **391** (1992) L1–L4.
- [4] F. Finelli and A. Gruppuso, “Resonant amplification of gauge fields in expanding universe,” *Phys. Lett. B* **502** (2001) 216–222, [arXiv:hep-ph/0001231](https://arxiv.org/abs/hep-ph/0001231).
- [5] A. L. Maroto, “Primordial magnetic fields from metric perturbations,” *Phys. Rev. D* **64** (2001) 083006, [arXiv:hep-ph/0008288](https://arxiv.org/abs/hep-ph/0008288).
- [6] A. L. Maroto, “Cosmological magnetic fields induced by metric perturbations after inflation,” in *5th International Conference on Particle Physics and the Early Universe*. 11, 2001. [arXiv:hep-ph/0111268](https://arxiv.org/abs/hep-ph/0111268).
- [7] S. Matarrese, S. Mollerach, A. Notari, and A. Riotto, “Large-scale magnetic fields from density perturbations,” *Phys. Rev. D* **71** (2005) 043502, [arXiv:astro-ph/0410687](https://arxiv.org/abs/astro-ph/0410687).
- [8] J. Martin and J. Yokoyama, “Generation of Large-Scale Magnetic Fields in Single-Field Inflation,” *JCAP* **01** (2008) 025, [arXiv:0711.4307 \[astro-ph\]](https://arxiv.org/abs/0711.4307).

- [9] V. Demozzi, V. Mukhanov, and H. Rubinstein, “Magnetic fields from inflation?,” *JCAP* **08** (2009) 025, [arXiv:0907.1030 \[astro-ph.CO\]](https://arxiv.org/abs/0907.1030).
- [10] S. Kanno, J. Soda, and M.-a. Watanabe, “Cosmological Magnetic Fields from Inflation and Backreaction,” *JCAP* **12** (2009) 009, [arXiv:0908.3509 \[astro-ph.CO\]](https://arxiv.org/abs/0908.3509).
- [11] K. Bamba and M. Sasaki, “Large-scale magnetic fields in the inflationary universe,” *JCAP* **02** (2007) 030, [arXiv:astro-ph/0611701](https://arxiv.org/abs/astro-ph/0611701).
- [12] K. Bamba, C. Q. Geng, and S. H. Ho, “Large-scale magnetic fields from inflation due to Chern-Simons-like effective interaction,” *JCAP* **11** (2008) 013, [arXiv:0806.1856 \[astro-ph\]](https://arxiv.org/abs/0806.1856).
- [13] N. Barnaby, R. Namba, and M. Peloso, “Observable non-gaussianity from gauge field production in slow roll inflation, and a challenging connection with magnetogenesis,” *Phys. Rev. D* **85** (2012) 123523, [arXiv:1202.1469 \[astro-ph.CO\]](https://arxiv.org/abs/1202.1469).
- [14] R. J. Z. Ferreira, R. K. Jain, and M. S. Sloth, “Inflationary magnetogenesis without the strong coupling problem,” *JCAP* **10** (2013) 004, [arXiv:1305.7151 \[astro-ph.CO\]](https://arxiv.org/abs/1305.7151).
- [15] P. W. Graham, J. Mardon, and S. Rajendran, “Vector Dark Matter from Inflationary Fluctuations,” *Phys. Rev. D* **93** no. 10, (2016) 103520, [arXiv:1504.02102 \[hep-ph\]](https://arxiv.org/abs/1504.02102).
- [16] R. Durrer and A. Neronov, “Cosmological Magnetic Fields: Their Generation, Evolution and Observation,” *Astron. Astrophys. Rev.* **21** (2013) 62, [arXiv:1303.7121 \[astro-ph.CO\]](https://arxiv.org/abs/1303.7121).
- [17] K. Subramanian, “The origin, evolution and signatures of primordial magnetic fields,” *Rept. Prog. Phys.* **79** no. 7, (2016) 076901, [arXiv:1504.02311 \[astro-ph.CO\]](https://arxiv.org/abs/1504.02311).
- [18] O. Özsoy and G. Tasinato, “Inflation and Primordial Black Holes,” *Universe* **9** no. 5, (2023) 203, [arXiv:2301.03600 \[astro-ph.CO\]](https://arxiv.org/abs/2301.03600).
- [19] S. Tripathy, D. Chowdhury, R. K. Jain, and L. Sriramkumar, “Challenges in the choice of the nonconformal coupling function in inflationary magnetogenesis,” *Phys. Rev. D* **105** no. 6, (2022) 063519, [arXiv:2111.01478 \[astro-ph.CO\]](https://arxiv.org/abs/2111.01478).
- [20] S. Tripathy, D. Chowdhury, H. V. Ragavendra, R. K. Jain, and L. Sriramkumar, “Circumventing the challenges in the choice of the nonconformal coupling function in inflationary magnetogenesis,” *Phys. Rev. D* **107** no. 4, (2023) 043501, [arXiv:2211.05834 \[astro-ph.CO\]](https://arxiv.org/abs/2211.05834).
- [21] B. Atkins, D. Chowdhury, A. Marriott-Best, and G. Tasinato, “Inflationary magnetogenesis beyond slow-roll and its induced gravitational waves,” [arXiv:2507.01772 \[astro-ph.CO\]](https://arxiv.org/abs/2507.01772).
- [22] G. Tasinato, “An analytic approach to non-slow-roll inflation,” *Phys. Rev. D* **103** no. 2, (2021) 023535, [arXiv:2012.02518 \[hep-th\]](https://arxiv.org/abs/2012.02518).
- [23] G. Tasinato, “Large — η — approach to single field inflation,” *Phys. Rev. D* **108** no. 4, (2023) 043526, [arXiv:2305.11568 \[hep-th\]](https://arxiv.org/abs/2305.11568).
- [24] L. Sorbo, “Parity violation in the Cosmic Microwave Background from a pseudoscalar inflaton,” *JCAP* **06** (2011) 003, [arXiv:1101.1525 \[astro-ph.CO\]](https://arxiv.org/abs/1101.1525).
- [25] C. Caprini and L. Sorbo, “Adding helicity to inflationary magnetogenesis,” *JCAP* **10** (2014) 056, [arXiv:1407.2809 \[astro-ph.CO\]](https://arxiv.org/abs/1407.2809).
- [26] K.-W. Ng, S.-L. Cheng, and W. Lee, “Inflationary dilaton-axion magnetogenesis,” *Chin. J. Phys.* **53** (2015) 110105, [arXiv:1409.2656 \[astro-ph.CO\]](https://arxiv.org/abs/1409.2656).
- [27] G. Tasinato, “A scenario for inflationary magnetogenesis without strong coupling problem,” *JCAP* **03** (2015) 040, [arXiv:1411.2803 \[hep-th\]](https://arxiv.org/abs/1411.2803).
- [28] K. Subramanian, “Magnetic fields in the early universe,” *Astron. Nachr.* **331** (2010) 110–120, [arXiv:0911.4771 \[astro-ph.CO\]](https://arxiv.org/abs/0911.4771).
- [29] R. Sharma, K. Subramanian, and T. R. Seshadri, “Generation of helical magnetic field in a viable scenario of inflationary magnetogenesis,” *Phys. Rev. D* **97** no. 8, (2018) 083503, [arXiv:1802.04847 \[astro-ph.CO\]](https://arxiv.org/abs/1802.04847).
- [30] D. Chowdhury, L. Sriramkumar, and M. Kamionkowski, “Enhancing the cross-correlations between magnetic fields and scalar perturbations through parity violation,” *JCAP* **10** (2018) 031, [arXiv:1807.07477 \[astro-ph.CO\]](https://arxiv.org/abs/1807.07477).

[31] S. Okano and T. Fujita, “Chiral Gravitational Waves Produced in a Helical Magnetogenesis Model,” [JCAP 03 \(2021\) 026](#), [arXiv:2005.13833 \[astro-ph.CO\]](#).

[32] A. Brandenburg, Y. He, and R. Sharma, “Simulations of Helical Inflationary Magnetogenesis and Gravitational Waves,” [Astrophys. J. 922](#) no. 2, (2021) 192, [arXiv:2107.12333 \[astro-ph.CO\]](#).

[33] S. Tripathy, D. Chowdhury, H. V. Ragavendra, and L. Sriramkumar, “Cross-correlation between the curvature perturbations and magnetic fields in pure ultraslow roll inflation,” [Phys. Rev. D 111](#) no. 6, (2025) 063550, [arXiv:2409.20232 \[astro-ph.CO\]](#).

[34] H. V. Ragavendra and L. Sriramkumar, “Observational Imprints of Enhanced Scalar Power on Small Scales in Ultra Slow Roll Inflation and Associated Non-Gaussianities,” [Galaxies 11](#) no. 1, (2023) 34, [arXiv:2301.08887 \[astro-ph.CO\]](#).

[35] N. Bhaumik and R. K. Jain, “Primordial black holes dark matter from inflection point models of inflation and the effects of reheating,” [arXiv:1907.04125 \[astro-ph.CO\]](#). [JCAP2001,037(2020)].

[36] H. V. Ragavendra, P. Saha, L. Sriramkumar, and J. Silk, “Primordial black holes and secondary gravitational waves from ultraslow roll and punctuated inflation,” [Phys. Rev. D 103](#) no. 8, (2021) 083510, [arXiv:2008.12202 \[astro-ph.CO\]](#).

[37] M. La Rosa and G. Tasinato, “Ultralight dark matter from non-slow-roll inflation,” [Phys. Rev. D 112](#) no. 12, (2025) 123542, [arXiv:2508.16455 \[astro-ph.CO\]](#).

[38] C. T. Byrnes, P. S. Cole, and S. P. Patil, “Steepest growth of the power spectrum and primordial black holes,” [JCAP 06](#) (2019) 028, [arXiv:1811.11158 \[astro-ph.CO\]](#).

[39] O. Özsöy and G. Tasinato, “On the slope of the curvature power spectrum in non-attractor inflation,” [JCAP 04](#) (2020) 048, [arXiv:1912.01061 \[astro-ph.CO\]](#).

[40] H. V. Ragavendra, A. K. Sarkar, and S. K. Sethi, “Constraining ultra slow roll inflation using cosmological datasets,” [JCAP 07](#) (2024) 088, [arXiv:2404.00933 \[astro-ph.CO\]](#).

[41] A. Talebian and H. Firouzjahi, “Axion ultraslow-roll inflation,” [Phys. Rev. D 112](#) no. 12, (2025) 123548, [arXiv:2507.02685 \[astro-ph.CO\]](#).

[42] L. Burmeister, P. Da Vela, F. Longo, G. Marti-Devesa, M. Meyer, F. Saturni, A. Stamerra, and P. Veres, “Constraints on the intergalactic magnetic field from Fermi-LAT observations of GRB 221009A,” [arXiv:2512.11128 \[astro-ph.HE\]](#).

[43] R. Durrer, L. Hollenstein, and R. K. Jain, “Can slow roll inflation induce relevant helical magnetic fields?,” [JCAP 03](#) (2011) 037, [arXiv:1005.5322 \[astro-ph.CO\]](#).

[44] F. R. Urban, “On inflating magnetic fields, and the backreactions thereof,” [JCAP 12](#) (2011) 012, [arXiv:1111.1006 \[astro-ph.CO\]](#).

[45] N. Bartolo, S. Matarrese, M. Peloso, and M. Shiraishi, “Parity-violating CMB correlators with non-decaying statistical anisotropy,” [JCAP 07](#) (2015) 039, [arXiv:1505.02193 \[astro-ph.CO\]](#).

[46] G. ’t Hooft, “A Planar Diagram Theory for Strong Interactions,” [Nucl. Phys. B 72](#) (1974) 461.

[47] C. Caprini and R. Durrer, “Gravitational wave production: A Strong constraint on primordial magnetic fields,” [Phys. Rev. D 65](#) (2001) 023517, [arXiv:astro-ph/0106244](#).

[48] A. Mack, T. Kahniashvili, and A. Kosowsky, “Microwave background signatures of a primordial stochastic magnetic field,” [Phys. Rev. D 65](#) (2002) 123004, [arXiv:astro-ph/0105504](#).

[49] G. Domènech, “Scalar Induced Gravitational Waves Review,” [Universe 7](#) no. 11, (2021) 398, [arXiv:2109.01398 \[gr-qc\]](#).

[50] D. Chowdhury, G. Tasinato, and I. Zavala, “The rise of the primordial tensor spectrum from an early scalar-tensor epoch,” [JCAP 08](#) no. 08, (2022) 010, [arXiv:2204.10218 \[gr-qc\]](#).

[51] A. Marriott-Best, D. Chowdhury, A. Ghoshal, and G. Tasinato, “Exploring cosmological gravitational wave backgrounds through the synergy of LISA and the Einstein Telescope,” [Phys. Rev. D 111](#) no. 10, (2025) 103001, [arXiv:2409.02886 \[astro-ph.CO\]](#).

[52] T. L. Smith, E. Pierpaoli, and M. Kamionkowski, “A new cosmic microwave background constraint to primordial gravitational waves,” [Phys. Rev. Lett. 97](#) (2006) 021301, [arXiv:astro-ph/0603144](#).

[53] **LISA Cosmology Working Group** Collaboration, P. Auclair *et al.*, “Cosmology with the Laser Interferometer Space Antenna,” *Living Rev. Rel.* **26** no. 1, (2023) 5, [arXiv:2204.05434 \[astro-ph.CO\]](https://arxiv.org/abs/2204.05434).

[54] **LISA** Collaboration, M. Colpi *et al.*, “LISA Definition Study Report,” [arXiv:2402.07571 \[astro-ph.CO\]](https://arxiv.org/abs/2402.07571).

[55] **ET** Collaboration, A. Abac *et al.*, “The Science of the Einstein Telescope,” [arXiv:2503.12263 \[gr-qc\]](https://arxiv.org/abs/2503.12263).

[56] T. L. Smith and R. Caldwell, “Sensitivity to a Frequency-Dependent Circular Polarization in an Isotropic Stochastic Gravitational Wave Background,” *Phys. Rev. D* **95** no. 4, (2017) 044036, [arXiv:1609.05901 \[gr-qc\]](https://arxiv.org/abs/1609.05901).

[57] R. Kato and J. Soda, “Probing circular polarization in stochastic gravitational wave background with pulsar timing arrays,” *Phys. Rev. D* **93** no. 6, (2016) 062003, [arXiv:1512.09139 \[gr-qc\]](https://arxiv.org/abs/1512.09139).

[58] **LISA Cosmology Working Group** Collaboration, J. E. Gammal *et al.*, “Reconstructing primordial curvature perturbations via scalar-induced gravitational waves with LISA,” *JCAP* **05** (2025) 062, [arXiv:2501.11320 \[astro-ph.CO\]](https://arxiv.org/abs/2501.11320).

[59] A. Ghaleb, A. Malhotra, G. Tasinato, and I. Zavala, “Bayesian reconstruction of primordial perturbations from induced gravitational waves,” *Phys. Rev. D* **112** no. 12, (2025) 123538, [arXiv:2505.22534 \[astro-ph.CO\]](https://arxiv.org/abs/2505.22534).

[60] N. Seto, “Prospects for direct detection of circular polarization of gravitational-wave background,” *Phys. Rev. Lett.* **97** (2006) 151101, [arXiv:astro-ph/0609504](https://arxiv.org/abs/astro-ph/0609504).

[61] N. Seto, “Quest for circular polarization of gravitational wave background and orbits of laser interferometers in space,” *Phys. Rev. D* **75** (2007) 061302, [arXiv:astro-ph/0609633](https://arxiv.org/abs/astro-ph/0609633).

[62] V. Domcke, J. Garcia-Bellido, M. Peloso, M. Pieroni, A. Ricciardone, L. Sorbo, and G. Tasinato, “Measuring the net circular polarization of the stochastic gravitational wave background with interferometers,” *JCAP* **05** (2020) 028, [arXiv:1910.08052 \[astro-ph.CO\]](https://arxiv.org/abs/1910.08052).

[63] N. M. J. Cruz, A. Malhotra, G. Tasinato, and I. Zavala, “Measuring the circular polarization of gravitational waves with pulsar timing arrays,” *Phys. Rev. D* **110** no. 10, (2024) 103505, [arXiv:2406.04957 \[astro-ph.CO\]](https://arxiv.org/abs/2406.04957).

[64] H. V. Ragavendra and N. Bartolo, “Twisted echoes of an odd quartet: Scalar-induced gravitational waves as a probe of primordial parity-violation,” [arXiv:2507.02733 \[astro-ph.CO\]](https://arxiv.org/abs/2507.02733).

[65] E. Dimastrogiovanni, M. Fasiello, A. Papageorgiou, and C. Z. Gatica, “Pure chromo-natural inflation: signatures of particle production from weak to strong backreaction,” *JCAP* **09** (2025) 042, [arXiv:2504.17750 \[astro-ph.CO\]](https://arxiv.org/abs/2504.17750).